School of Mechanical and Manufacturing Engineering

Faculty of Engineering

UNSW Sydney

Multi-objective Design Optimisation of Coronary Stents

By

Vanessa Luvio

Thesis submitted as a requirement for the degree of Bachelor of Mechanical Engineering

Submitted: 20 November 2020 Student zID: z5164214
Supervisor: Dr Susann Beier (UNSW)

ORIGINALITY STATEMENT

'I hereby declare that this submission is my own work and to the best of my knowledge it contains no materials previously published or written by another person, or substantial proportions of material which have been accepted for the award of any other degree or diploma at UNSW or any other educational institution, except where due acknowledgement is made in the thesis. Any contribution made to the research by others, with whom I have worked at UNSW or elsewhere, is explicitly acknowledged in the thesis. I also declare that the intellectual content of this thesis is the product of my own work, except to the extent that assistance from others in the project's design and conception or in style, presentation and linguistic expression is acknowledged.'

Signed 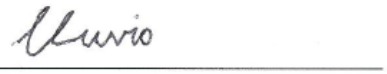

Date 19/11/2020

Abstract

In-stent restenosis remains a major problem in coronary stent design and is caused by mechanical failure and stent-induced, adverse effects on the local haemodynamic environment. A multi-objective optimisation of stent design was completed for eight major stent design variables and three key stent performance objectives. Latin Hypercube sampling generated an initial set of 30 novel stent designs, which were computationally modelled for their haemodynamic and mechanical performance using CFD and FEA respectively. The results were then used to inform an optimisation algorithm, NSGA-II with EHVI, to predict non-dominated / ideal stent designs. Directly contributing to a journal submission, 22 non-dominated stents were identified. Key findings included the more favourable haemodynamic performance of circular-strutted stents, the trade-off between cell height and strut thickness, and the effect of the number of connectors on radial and compressive strength. Substantial progress was made towards future work by expanding the number of variables and objectives.

Acknowledgements

I would like to express my deep gratitude to my thesis supervisor, Dr Susann Beier, for her valuable insight, guidance, constructive critiques, and support while overseeing my thesis. I would also like to sincerely thank Mr Ramtin Gharleghi for his time and expertise in using the available resources. In addition, I would like to extend my grateful thanks to Mr Somesh Khullar and Mr Anushan Senthurnathan for assisting me in obtaining the available resources, to Mr Tejas Canchi for his guidance with the FEA modelling, and to Mr Matthew Eyles for his continued support and assistance throughout my entire thesis. I would also like to thank Mr Behzad Babaei and Mr Gangadhara Prusty for reviewing my FEA setup and assisting with technical errors, and to Dr Ray Tapabrata for his multi-objective optimisation code that was used in this study.

This study was completed with the assistance and services provided by Katana, a shared computational cluster at UNSW. My grateful thanks go to the staff operating Katana and for their quick responses and assistance when requested.

Contents

List of Figures

List of tables

Nomenclature

a	*Yasuda Exponent*
A_1	*Inlet Area*
A_s	*Surface Area*
C	*Damping Matrix*
D	*Stent Diameter*
D_1	*Initial Stent Diameter*
D_2	*Final Stent Diameter*
f	*Body Force in CFD*
F	*Applied Force in FEA*
i	*Iteration*
K	*Stiffness Matrix*
l	*Acting Bending Length*
M	*Mass Matrix*
n	*Index*
p	*Pressure in CFD*
P	*Applied Pressure in FEA*
r	*Distance from r_{max} to Vessel Centreline*
r_{max}	*Vessel Radius*
t	*Time*
u	*Displacement vector*
v	*Flow Velocity*
v_{avg}	*Average Velocity*
v_{max}	*Velocity at the Vessel Centreline*
μ_a	*Apparent Viscosity*
δ	*Deformation*
ρ	*Density*
Δ	*Divergence*
μ_D	*Dynamic Viscosity*
μ_0	*Constant Viscosity*
μ_∞	*High Shear Viscosity*
γ	*Newmark Accuracy Control Variable*
β	*Newmark Stability Control Variable*
λ	*Time Constant*
$\dot{\gamma}$	*Shear Strain Rate*
Δt	*Time Step*
AT	*Alignment Type*
CH	*Cell Height*
CT	*Connector Type*
ISR	*In-stent Restenosis*
NC	*Number of Connectors*
ND	*Non-Dominated*
NP	*Number of Peaks*
PCI	*Percutaneous Coronary Intervention*
Re	*Reynolds Number*
SA	*Intra-Strut Angle*
SD1	*Strut Dimension 1*
SD2	*Strut Dimension 2*
TAWSS	*Time Averaged Wall Shear Stress*
TLR	*Target Lesion Revascularisations*
WSS	*Wall Shear Stress*

Chapter 1 - Introduction

1.1. Coronary Artery Disease

The development of coronary stents has provided a significant source of treatment for cardiovascular disease, the greatest cause of death in the modern world. Cardiovascular disease encompasses multiple diseases including coronary artery disease which involves atherosclerosis [1]. Atherosclerosis is described as the build-up of plaque, made of fats such as cholesterol, that thickens and hardens in the artery and prevents blood flow [2]. This built-up plaque consequently narrows the space inside the artery called the artery lumen, and this process is known as restenosis. Coronary artery disease is caused by multiple factors including having a genetic predisposition to the disease, high blood pressure, and lifestyle factors such as having a poor diet. This disease has killed 9.43 million people globally in 2016 alone making coronary stent treatment vitally important.

Percutaneous coronary intervention (PCI) is a highly effective technique for the treatment of coronary artery disease. PCI involves the delivery of a stent to the point of occlusion via a catheter inserted into a patient's artery and balloon angioplasty. The stent is mounted to a balloon which inflates, stretching the vessel wall and expanding the stent. The stent is a tubular scaffold which is designed to stay expanded, push back the plaque and thereby increase the lumen diameter of the artery for increased blood-flow (Figure 1). It is a popular choice of treatment due to it being less invasive than surgery, having faster in-hospital recovery and reduced costs [1]. The other treatments available for stenosis are drug treatment and surgery. Drug treatment can be used for less severe cases and can develop a drug dependency in patients. Alternatively, bypass graft surgery is predominantly used in severe cases due to its high mortality rate, invasiveness and cost [3]. One adverse result of PCI is the development of in-stent restenosis where the artery is narrowed again due to cell overgrowth in or around the stent. The development of drug-eluting stents has successfully reduced in-stent restenosis to less than 10% [1] however some patients will need surgical interventions, especially for repeat, recalcitrant in-stent restenosis cases [4].

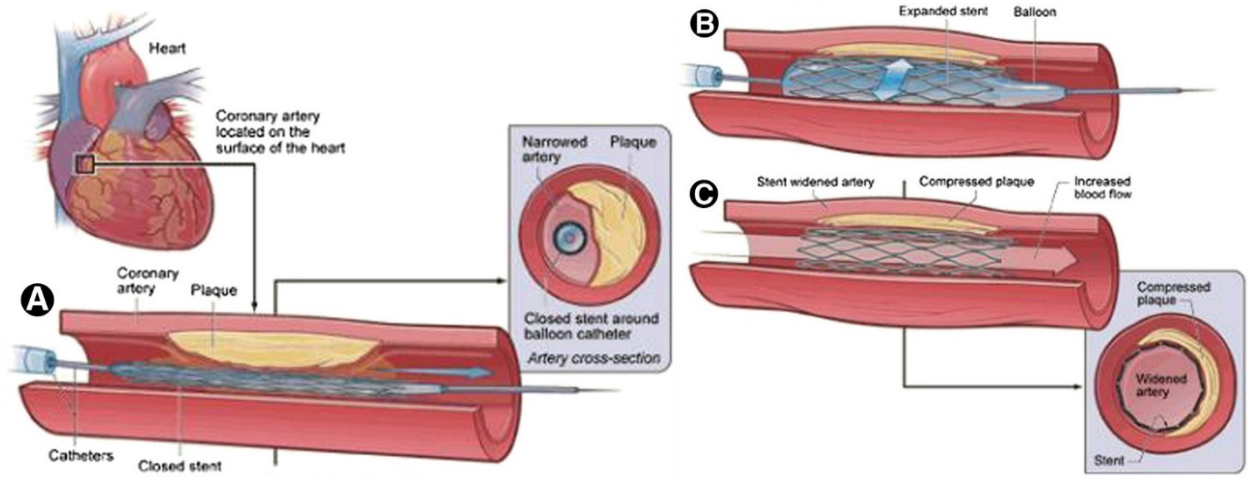

Figure 1. Percutaneous Coronary Intervention with Stent Implantation (A to C) [5].

To address the issue of in-stent restenosis for PCI, there have been multiple developments in stent design. In 1986, the first coronary stent was implanted by Sigwart and Puel which successfully reduced the vessel recoil and restenosis experienced by patients that underwent balloon angioplasty [6]. However, the bare metal stents at the time generated other issues including in-stent restenosis, stent thrombosis, deployment failure and embolization. Drug-eluting stents were developed to reduce in-stent restenosis and the first sirolimus-eluting stents were implanted in 1999. Known as the first generation of drug-eluting stents, these stents successfully reduced in-stent restenosis however increased the risk of stent thrombosis. Bare metal stents and second-generation everolimus-eluting drug-eluting stents continue to be refined in material composition and stent design to address these issues.

1.2. Failures of Percutaneous Coronary Intervention

1.2.1. In-Stent Restenosis and Adverse Effects on the Haemodynamic Flow

In-stent restenosis (ISR) remains a major problem for percutaneous coronary intervention (PCI) despite improvements in stent design. Studies have shown that ISR has an incidence rate between 17% and 41% for bare-metal stents. While drug-eluting stents improve upon this with 5% to 10% incidence of ISR, there is large concern for these stents and their delayed endothelialisation causing late thrombosis [7] [8]. Stent thrombosis is the formation of blood clots inside the stent, creating a point of occlusion for the blood flow, and it is a key determinant of stent failure causing death with mortality ranging between 11% and 45% [9]. A principle cause of ISR is neointimal hyperplasia which is the development of vascular muscle cells as a response to injury in the vessel wall. This occurs during stent implantation, and an excessive amount will thicken the arterial wall causing ISR [3]. Target lesion revascularisation (TLR) is then performed to restore the blood flow. There are multiple factors that influence the development of ISR including patient-specific factors such as the lesion types, medical history and reaction to the drug, as well as stent design factors such as mechanical failure and a stent's adverse effects on the local haemodynamic environment [7].

Flow disturbances have been shown to influence neointimal growth resulting in restenosis and thrombus formation [10]. Specifically, areas of low wall shear stress (WSS) and oscillatory WSS have been identified as areas where the most intimal thickening occurs. WSS is the shear stress located at the wall of the vessel, induced by the tangential drag force from the blood flow. The haemodynamic flow is altered by the stent-induced biological response. Studies have highlighted the significance of stent design and haemodynamics for the development of ISR, however, the majority have focussed on strut thickness and spacing. Hence, there is a need for further development in stent design in relation to the haemodynamic environment [8]. Atherosclerosis is the adverse result of changes to haemodynamic flow. Metrics to describe this change and its effects have been well-established and include wall shear stress (WSS), and time-averaged WSS (TAWSS) [11];

Time-Averaged Wall Shear Stress (TAWSS)

Averaging the WSS over the cardiac cycle will determine TAWSS. It accounts for the change in haemodynamic flow through time. Low TAWSS has been connected to endothelialisation, which is the formation of tissue made of cells that line the vessel. Cellular proliferation, inflammation and intimal are linked to areas with TAWSS < 0.5 Pa [12].

Wall Shear Stress (WSS)

Relatively low WSS has been shown to promote intimal thickening and exist in locations of atheromatous disease. Specifically, intimal hyperplasia has developed at locations where WSS < 1.5 Pa due to the release of tissue growth factors. The same study [13] commented that areas with WSS < 0.5 Pa are prone to atherosclerosis, yet the plaque in these locations was stable and stiffer. This atheromatous narrowing was shown to decrease for areas of WSS > 1.2 Pa. Given its significant association with the formation of neointimal hyperplasia, low wall shear stress has been of specific interest in stent design studies and is defined to occur in areas where WSS < 1 Pa [14]. However, investigations into high WSS have also indicated an adverse response with an increased risk in thrombosis and plaque rupture. Specifically, a more vulnerable disease phenotype with plaque vulnerable to rupture is suggested to develop in areas where WSS > 2.5 Pa [15]. Typically, high wall shear stress has been defined to occur in areas where the WSS > 3 Pa [16]. Hence, there are adverse patient outcomes and risk associated with both high and low WSS.

1.2.2. Mechanical Failure of Coronary Stents

Stent struct fracture can develop adverse clinical outcomes including neointimal hyperplasia, thrombus occlusion, the proliferation of scar tissue, and ISR [17]. Therefore, it is crucial to design stents with strong, mechanical integrity to avoid fracture. To determine what aspects need to be optimised, the factors that contribute to ISR were considered. These are stent elastic recoil which narrows the lumen diameter, stent-induced damage to the arterial wall during expansion, stent recoil or vessel movement, and stresses generated in the vessel wall causing arterial remodelling [18].

There are multiple mechanical forces acting on a stent including compression, torsion, flexion and elongation [19]. Stent failure and fracture can occur from a combination of these forces, either during delivery in the arteries or at the diseased arterial location. Based on these forces, the optimal stent design should minimise elastic recoil, fracture and injury to the vessel wall by guaranteeing sufficient longitudinal and radial strength. Moreover, the design should ensure flexibility for efficient deliverability during surgery, and reduce tissue prolapse with a strong dense mesh [18]. Stent design has a crucial role in minimising stent fracture, however, some variables benefit the stent in one way but are detrimental to another objective. There is a need for balance between radial strength, longitudinal strength and flexibility which are required to achieve the optimal stent design [17].

1.3. Design of Coronary Stents

Stent design has significantly developed since its inception in the 1980s. There is currently a large variety of commercial stents available however there are opportunities for design improvement. Reducing the rate of ISR in patients has been heavily investigated by addressing key areas of mechanical failure and stent-induced, adverse effects on the haemodynamic environment [20]. There are multiple factors that influence stent design, however, the most significant developments have been in stent material choice, strut size and connector geometry. Multiple studies have used computational simulations to evaluate stent design variables and their effect on mechanical and haemodynamic outcomes. Yet, there is no clear optimal stent design due to the complex relationship between stent variables and design objectives.

Chapter 2 - Literature Review

This chapter provides a review, discussion and analysis of key literature with relevance to stent design variables, key areas of optimisation, and computational modelling with finite element analysis and computational fluid dynamics.

2.1. Significant Stent Design Variables

Stent design has a significant effect on minimising adverse haemodynamic outcomes and mechanical failure which can cause ISR. Different current commercial stent designs are pictured in Figure 2, and the following section discusses literature that investigates key stent design features.

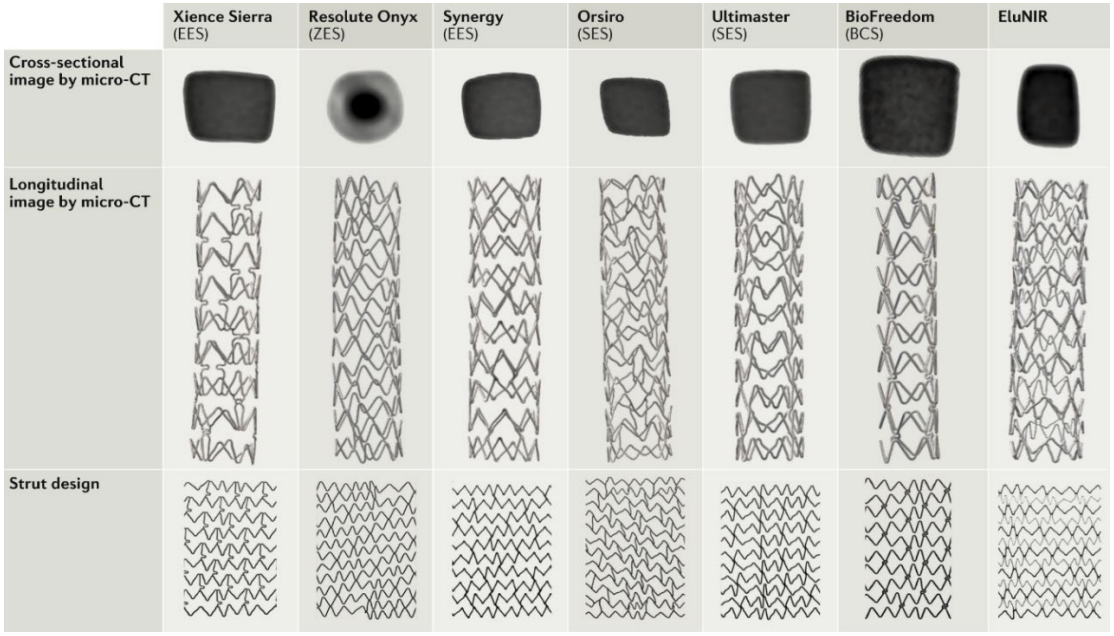

Figure 2. Current Commercial Stents [21].

2.1.1. Connector Geometry and Hoop Alignment

The connectors are the struts that connect the stent cells together and provide the stent's longitudinal strength and flexibility. Pant et al. [8] compared five commercial stent designs and found that the length of connectors in the cross-flow direction is proportional to the areas of adverse low WSS and recirculation zones which can lead to restenosis. Upon analysis, this study highlighted the relatively high WSS found at the proximal end of all the stents and the areas of low WSS found localised around the struts. Both Pant et al. and He et al. [22] concluded that curve-shaped connectors disturb the haemodynamic flow more than straight connectors, and that connectors should be aligned longitudinal to the flow to be haemodynamically beneficial. This study by He et al. provided a parametric optimisation of four commercial stents and highlighted that thrombosis and neointimal hyperplasia could be reduced by reducing the number of strut connectors to the minimum required for sufficient mechanical integrity. In contrast, a meta-analysis of 53 studies [10] found that stents with a higher average number of connectors, greater than 2.5, were linked to a lower incidence of stent thrombosis and TLR. Moreover, the study found that there was a need for connectors at the proximal and distal edges for longitudinal integrity.

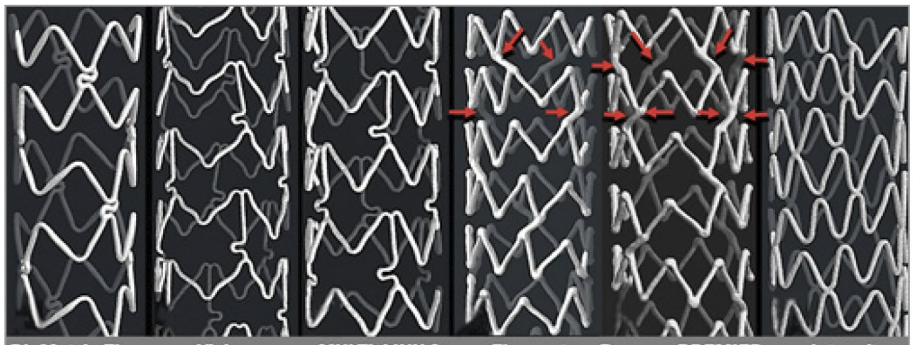

BioMatrix Flex	Vision	MULTI-LINK 8	Element	Promus PREMIER	Integrity
Stainless steel	Cobalt chromium L605	Cobalt chromium L605	Platinium chromium	Platinium chromium	Cobalt nickel MP35M
120 µm	81 µm	81 µm	81 µm	81 µm	91 µm
2 connectors	3	3	2	2 (4 between proximal hoops)	2-3

Figure 3. Commercial Stent Designs (Some Connectors are Indicated by Red Arrows) [17].

With a focus on deliverability, radial strength and conformability, many commercial designs have reduced their longitudinal strength. Providing a comparison of the commercial stents pictured in Figure 3, one study [20] found that the longitudinal integrity of stents was closely linked to the hoop strength, and the geometry, number and alignment of the connectors. Longitudinal deformation can prompt stent thrombosis and this deformation at the proximal end of stents is likely to occur from equipment catching [20]. Moreover, the study highlighted that the connector alignment between rings will impact the stent's longitudinal integrity. The two most common alignment types are 'peak to peak' or 'peak to valley,' such as the Vision (Abbot Vascular) stent and Biomatrix Flex (Biosensors) stent respectively, pictured in Figure 3.

The commercial stent designs illustrated in Figure 3 were originally investigated with a repetitive bend test in the study by Ormiston et al [17]. Both studies concluded that the CYPHER (Cordis Corporation) stent experiences the most fracture because of its six thick connectors making it less flexible and deliverable despite its strength. Of the six designs tested, there was a range of connector geometries including S-shaped (BioMatrix Flex), off-set peaks linked by a straight connector (Element and Promus PREMIER), and connectors with a U-shaped loop (Vision and MULTI-LINK 8). Ormiston et al. showed that curved sections of connectors are where most fractures occurred due to stress concentrations, however, the flexibility of the stent is increased by these bends in the connectors. Similarly, a later study [23] confirmed that straight connectors had higher longitudinal strength than curved connectors (S-shaped). The authors highlighted that increasing the number of connectors will improve and increase the stent's longitudinal strength. Specifically, the FEA models showed that the stent with four connectors provided nearly three times as much longitudinal strength as a stent with two connectors. In contrast, Ormiston et al. provides the view that two connectors create flexible stents that are less likely to fracture than those with more connectors. Commercially, current stents have between two to three connectors between hoops, except for Promus Premier with has four connectors in its proximal hoops to improve longitudinal integrity.

2.1.2. Cross-Sectional Shape

The cross-sectional shape of stent struts can have a direct impact on flow patterns in the haemodynamic environment and on the stent's mechanical strength and susceptibility to fracture. One study [24] reported that the cross-sectional shape must be chosen to create a stent design with sufficient strength and considers the struts interaction with the vessel wall. In literature, suitable strut cross-sectional shapes identified include triangular, rectangular and circular [24] [25]. Of particular concern to multiple studies is the effect that strut cross-sectional shape has on the haemodynamic environment, creating flow separation and recirculation zones, producing low WSS. A 3D multi-objective study by Putra et al. [26] concluded that triangular struts were superior to rectangular struts due to their streamlined shape resulting in reduced flow disturbance. A streamlined cross-sectional shape has been shown to reduce recirculation zones and low flow shear rates [25]. Another study [27] showed that circular cross-sections reduce the level of flow fluctuations when compared to square struts. However, from a strength perspective, square cross-sections can tolerate a larger buckling force before failure [28]. Hence the balance between haemodynamic and mechanical objectives on strut cross-sectional shape needs to be carefully considered.

2.1.3. Stent Diameter

In vivo, patient-based studies have largely reported that increasing the stent diameter decreases the risk of ISR. One study [29] analysed the effect of stent diameter on adverse patient outcomes by analysing patient data collected from January 2010 to December 2016. The authors found that the TLR rates decreased from 7.2% to 3.3% as the diameter increased based on their analysis of four stent diameter sizes including diameters $\leq$ 2.50mm, 2.75 $\leq$ 3.00mm, 3.25 $\leq$ 3.50mm, and $>$ 3.50mm. The $<$ 2.50mm group produced the highest rates of major adverse cardiac events including death. Grouping patient results based on diameter was also completed by a separate study [30] that focussed on a diameter of 2.5mm or greater than 2.5mm. Similarly, the authors highlighted the higher rate of TLR and myocardial infarction, known as heart attacks, for the 2.5mm stents however commented that the rates of stent thrombosis were largely unaffected by the stent diameter. Moreover, one study [31] concluded that high rates of ISR, stent thrombosis and TLR occur in small vessels and suggested that there was a benefit in oversizing drug-eluting stents in smaller vessels.

The effect of larger stent diameters for bare-metal stents and drug-eluting stents has been largely debated. One study [32] investigated this by comparing data from 466 patients using drug-eluting stents or bare-metal stents with arteries $\geq$ 3.50mm. For large coronary arteries, the authors concluded that there was no added benefit in using drug-eluting instead of bare-metal stents, noting that stent thrombosis did not occur for either stent type and that larger vessels could manage larger neointimal growth before needing TLR. However, a later study [33] disagrees with this finding by highlighting that the strongest predictor of ISR is from using bare-metal stents even in patients with a stent diameter $\geq$ 3mm. Specifically, for every 1mm increase in diameter, the study showed a 76% lower risk of ISR. There are few studies that investigate stent diameter through parametric optimisation, and instead, most analyse patient results.

2.1.4. Number of Peaks and Intra-strut Angle

The number of peaks and the intra-strut angle are inter-related in their effect on the haemodynamic environment. The number of peaks is the number of high points in the sinusoidal curve per stent cell (Figure 5), and the intra-strut angle is illustrated in Figure 4. A study by Gundert et al. [34] used parametric computational optimisation and found that the intra-strut angle determined the optimal number of peaks in terms of reducing low TAWSS. Specifically, an intra-strut angle between 38.5 degrees and 46 degrees was shown to minimise the area of low TAWSS and to be independent of vessel diameter. However, the same author revised the optimal intra-strut angle, specifying that it should be within 50 degrees and 60 degrees in later work [35]. Moreover, different ranges of optimal intra-strut angles were found for different stent diameters with a different number of peaks, suggesting these three design variables are linked and require further investigation.

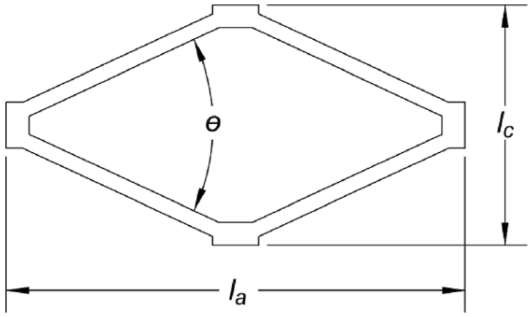

Figure 4. Cell design used by Gundert et al. where θ is the intra-strut angle [34].

In the later study by Gundert et al. [35], it was found that while stents need an increased number of peaks as diameter increases (due to expansion), reducing the number of peaks in current commercial designs would be haemodynamically beneficial. Nonetheless, the same study found that fewer peaks causes flow misalignment and adversely affects TAWSS. This phenomenon was also observed by a separate study [11] when comparing TAWSS results from the 9-peak Biomatrix (Biosensors) and 8-peak Omega (Boston Scientific) stent design. In contrast, a meta-analysis [10] was conducted that determined that the number of peaks had a minimal impact on stent thrombosis and TLR. Though minimal, an average number of peaks < 7.5 did not perform as well in terms of stent thrombosis and current commercial stents have been shown to have a number of peaks ranging from six to nine.

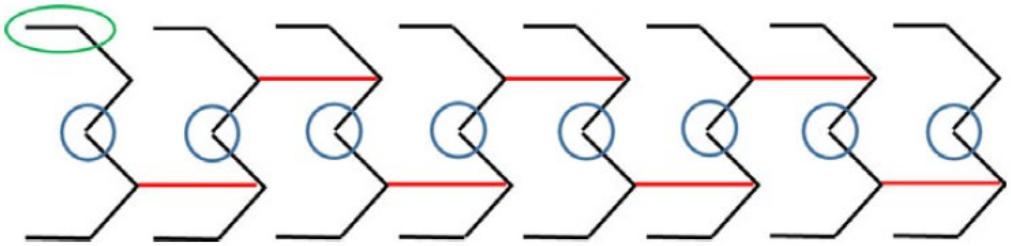

Figure 5. Diagram of Stent Connectors (Red), the Strut Thickness (green), and Peaks (blue) [10].

2.1.5. Strut Dimensions

Strut thickness has a significant effect on wall shear stress and must be considered when determining a stent's mechanical strength. One study [20] discussed the development of strut thickness through history. Originally, thick stainless-steel struts, as seen in the CYPHER, determined its strength, and recently, the development of alloys including cobalt-chromium, have enabled thinner struts with adequate radio-opacity and radial strength. Commercial designs offer a range of thicknesses, the smallest being 60 μm (Supraflex) and the largest being 140 μm (CYPHER) [25]. Thickness and width define the strut's dimensions as illustrated in Figure 6. One study [2] highlighted that stent radial strength is majorly dictated by strut width, while thickness is connected to ISR. Similarly, a separate study [36] observed a significant reduction in restenosis for thinner struts when comparing thick 140 μm struts to 50 μm struts in an analysis of 651 patients. Reducing strut thickness is largely agreed upon as beneficial for deliverability and reducing disturbances on the haemodynamic environment. Specific to WSS, Beier et al. [11] found that thinner struts resulted in higher WSS between cells and a reduction in low, adverse TAWSS. It is evident that thinner struts are beneficial to the haemodynamic environment but must take into account mechanical strength as well.

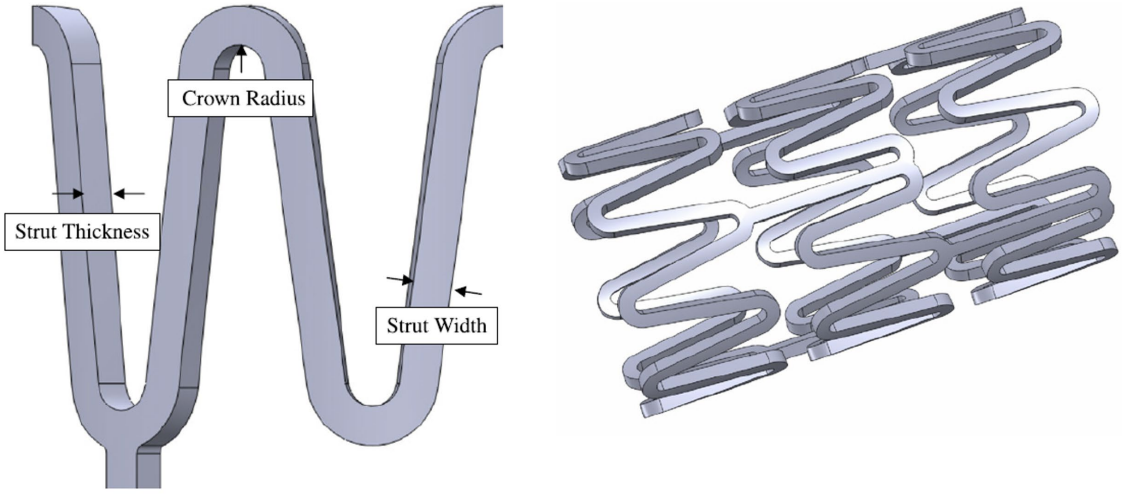

Figure 6. Strut Thickness and Width [2].

2.1.6. Cell Height

The vertical distance between stent cells is the cell height and this variable has been shown to affect the haemodynamic environment. Beier et al. [11] has suggested that there is a relationship between cell height and strut size. The study reported areas of low WSS and high WSS gradient for stents with a narrow cell height. Importantly, the authors found that decreasing the strut size would reduce these areas of adverse flow for stent designs with narrow cell height. Larger spacing (cell height) has shown to be beneficial to haemodynamic flow due to the increase in intra-strut area, reducing the stress experienced across the stent [37]. A later study [26] highlighted that cross-sectional shape and cell height are linked and both have an effect on the haemodynamic environment. Hence, analysis of the haemodynamic effects from cell height must also consider the effect of strut cross-sectional shape and strut size.

2.2. Optimisation of Coronary Stent Design

2.2.1. Mechanical Optimisation Objectives

Multiple studies have investigated the mechanical properties of coronary stents for the purpose of minimising adverse clinical outcomes. A study by Hsaio et al. [2] developed computational models representing variants of commercial stents with the purpose of measuring radial strength, expansion recoil, plastic strain, and the pulsatile fatigue safety factor. Measuring the strain experienced by commercial stents was similarly completed by an earlier study [19] but the torsion in addition to bending and compression was examined. This study focussed on the connection between strain zones and stent fracture, while Hsaio et al. examined plastic strain and expansion recoil to determine the radial strength of the stents.

Deliverability, flexibility and radial strength have been the objective focus of multiple designs, which has led to negative impacts on a stent's longitudinal strength. This view is evident in one study [38] which analysed patient angiographic results between September 2007 and September 2011 and identified longitudinal stent deformation. It was determined that the development of thin struts had sacrificed longitudinal strength, increasing the risk of thrombosis, and that it was unlikely due to procedural technique. Conversely, one study [39] stressed the occurrence of fracture during the delivery procedure through the analysis of 1000 patients and bench testing. Bench testing has proven to be a common practice for investigating the relationship between stent flexibility and fracture in multiple studies [17] [40]. The effect of 2-link and 3-link connectors on flexibility has been specifically examined by measuring and analysing the angles at the diastole and systole ends [40]. In contrast to this quantitative method, the other study [17] visually inspected the fractures that developing in the commercial stents from the bench testing.

2.2.2. Haemodynamic Flow Optimisation Objectives

When designing stents to benefit haemodynamic flow, a common objective across all literature is minimising areas of low wall shear stress (WSS). A study by Pant et al. [8] compared five commercial stent designs with CFD to investigate different stent designs and their effect on abnormal flow features including low WSS and oscillating WSS which are usually more susceptible to restenosis. Unlike other studies, this study focused on strut thickness and spacing, and examined the effect of these variables and connectors by quantifying the WSS patterns and flow features with a modified oscillatory shear index. Likewise, a later study [35] also investigated variants of commercial stent designs by completing 21 optimisations to minimise the area of stent-induced low WSS and TAWSS. This study instead focussed on the relationship between two variables, the number of crowns and stent diameter, and used the intra-strut angle to quantify results.

While both of these CFD studies assumed Newtonian flow, Beier et al. [11] offered an extensive investigation into two commercial stents while assuming non-Newtonian flow which provided more accurate near-wall results. This study considers more haemodynamic objectives than previous studies' focus on low WSS and TAWSS by including high WSS and WSS gradient using well-established metrics. Using these metrics, the author compared key stent design features (strut spacing, strut size, protrusion, and cell height) to examine their effect on a stent's haemodynamic profile.

2.2.3. Coronary Artery Stent Design Improvement Process

Multiple studies have attempted to improve stent design based on these mechanical and haemodynamic objectives through systematic computational optimisation. A study by Bressloff et al. [41] provides a thorough overview of the computational optimisation methods used in many of these studies with a particular focus on multi-objective methods. As an overview, there are four key elements to all optimisation methods; the design variables, the objective function, the constraints, and the optimisation algorithm. While initial studies focused on the optimisation of stents based on a single objective [34] [42] [43] [44], recent studies have considered multiple objectives, either from creating a single weighted objective function [45] or from treating each objective separately and creating a Pareto front; a set of non-dominated solutions. A surrogate modelling approach, which represents the relationship between stent design variables and the objection function, has been used in the majority of stent optimisation studies, ultimately creating the Pareto front in a time-efficient manner. Significantly, this study emphasised that the method of Kriging was the predominant method used in surrogate modelling.

The majority of stent optimisation studies have focused on mechanical optimisation and consider between three to four design variables [42] [45] [46] [47] [48]. Of these design variables, strut width and thickness are considered the most, and of the objectives considered in these studies, the radial strength is assessed by all. There are few studies that optimise coronary stents based on their effect on the haemodynamic environment. Of those that do, the vast majority consider a single objective and this is often reducing low WSS [34] [43] [44]. Commonly used in stent optimisation, Latin Hypercube sampling samples the design space efficiently [46] [48]. Similar space-filling methods used in these studies include LPτ sampling [47] and the Modified Grid Sampling approach [42]. While one study [45] provided a parametric multi-objective optimisation based on a single weighted objective function, the majority of stent optimisation studies used Kriging surrogate models and varied in their optimisation algorithms. Specific optimisation algorithm methods used in these studies to generate Pareto fronts include the Multiobjective Particle Swarm Optimisation algorithm [48], and the non-dominated sorting genetic algorithm called NSGA-II [46] [47] [49]. To rank the designs, NSGA-II has used the fitness function called Expected Hypervolume Improvement (EHVI) in multiple studies [26] [44].

There are minimal studies investigating the effect of a stent's design on minimising both mechanical and haemodynamic adverse clinical outcomes. A study by Pant et al. [49] considered both mechanical and haemodynamic objectives in the optimisation of the CYPHER (Cordis Corporation, Johnson & Johnson co.) stent with three design variables and six objectives. This study developed Kriging response surface models and used NSGA-II to search for an optimal set of designs (non-dominated solutions). Using this multi-objective optimisation process, conflict was identified between pairs of objectives such as the haemodynamic disturbance and flexibility of a stent. Similarly, a study by Putra et al. [26] considered both haemodynamic and mechanical objectives using Kriging response surface models, however, looked at only two design variables and fewer objectives (two); minimising low WSS, and minimising initial average stress. Building on from the authors' previous single objective study [44], optimal designs were searched for using the Expected Hypervolume Improvement algorithm (EHVI). Providing an extensive review of literature, one study [50] highlighted that stent design needs to consider the impact of mechanical strut support and

the vessel response to blood flow, in order to minimise ISR. Most literature investigates stent designs in relation to either haemodynamic flow behaviour or mechanical integrity and considers less than four design variables. Hence, this area of research into stent design optimisation can be expanded by considering both haemodynamic and mechanical outcomes for more variables with Kriging Surrogate modelling and using optimisation algorithms such as NSGA-II.

2.3. Computational Modelling of Stents with Finite Element Analysis

Computational simulations using finite element analysis (FEA) can evaluate a given structure and determine the mechanical reaction to various loading and boundary conditions that can imitate real-world environments. Multiple studies have modelled stents and utilised FEA to analyse their mechanical response to specific loading conditions that can cause stents to fail. FEA is highly beneficial to mechanical stent design optimisation, providing a rapid and extensive evaluation of multiple designs in an efficient, cost-effective manner with highly controlled conditions. The reliability of these results is largely dependent on the assumptions made for the model set-up.

Using FEA, multiple mechanical stent design objectives including stress, strain and displacement can be solved for by deriving equations that link these properties together. Based on the simple boundary conditions and low deformation rate associated with modelling stents in literature, the appropriate numerical approach was determined to be the implicit finite element method. One study [51] highlighted that this method has proven to be efficient specifically when solving equations with material non-linearities, which has been highlighted as a key difficulty when simulating stent expansion [52]. A stent can be studied using computational static structural analysis that contains the stiffness-based implicit time integration algorithm using the Newmark method. The implicit equation is incrementally solved throughout a given time. Firstly, the semi-discrete equation of motion is defined as follows;

$$M\ddot{u} + C\dot{u} + Ku = F \tag{1}$$

The Newmark time integration method is used for implicit transient analysis and assumes the equation can be represented by:

$$M\ddot{u}_{i+1} + C\dot{u}_{i+1} + Ku_{i+1} = F_{i+1} \tag{2}$$

The derived displacement vector is defined as:

$$u_{i+1} = u_i + \Delta t\dot{u}_i + \frac{\Delta t^2}{2}[(1-2\beta)\ddot{u}_i + 2\beta\ddot{u}_{i+1}] \tag{3}$$

The derived velocity vector is defined as:

$$\dot{u}_{i+1} = \dot{u}_i + \Delta t[(1-\gamma)\ddot{u}_i + \gamma\ddot{u}_{i+1}] \tag{4}$$

Where u is the displacement vector, $\dot{u}$ is the velocity vector, $\ddot{u}$ is the acceleration vector, i is the iteration, t is time, Δt is the time step, F is the applied force, M is the mass matrix, C is the damping matrix, K is the stiffness matrix, β is the Newmark stability control variable, and γ is the Newmark accuracy control variable.

While this procedure is unconditionally stable and efficient, it does contain limitations. For a complex model with complicated contact conditions, the computational time required to solve the simulation will increase, despite the number of equations staying the same [51]. Complex geometries will require extremely refined mesh, consequently increasing the computational time and power required. Therefore, mesh convergence studies are completed to achieve accurate results while considering the computational cost. Studies have emphasised that with every calculation there is an accumulation of computational error impacting on the accuracy of the results [18]. While there are limitations, FEA has proved to provide a good approximation to stents performance in real-life conditions given accurate modular setup is provided. Studies devoted to using FEA for stent evaluation attempt to replicate the actual stent and arterial environment through carefully chosen model geometry, mesh size, and boundary and loading conditions.

2.3.1. Geometry and the Numerical Model

The numerical model is a part of the FEA process, and its purpose is to create geometry that closely relates to real-life conditions. A study by Migliavacca et al. [52] provided a parametric analysis on 8 modelled stents using FEA. The results showed that the stent's geometry has a significant impact on the stents mechanical response to expansion and recoil. The authors proposed that modelling the arterial vessel and plaque and simulating contact with the stent would provide a more accurate analysis of its mechanical behaviour. Similarly, a later study [53] also emphasised the significance of replicating real-life conditions. The authors used in vitro static loading experiments to provide experimental verification for their FEA results measuring stent deformation and stress/strain distributions. Hence, to validate and improve the reliability of the analysis, stent geometry should initially be modelled to represent designs that have been tested and have experimental data for comparison.

2.3.2. Meshing Structure

The finite model geometry is discretised into mesh elements and the solver derives values for each element. The process of refining the mesh and the chosen mesh type is significant and is largely determined by the complexity of the geometry. Multiple studies have specifically used linear hexahedral elements and completed a mesh sensitivity study to examine the effect of mesh size on the simulated results [53] [54]. Moreover, one study in particular [53] highlighted that refining the mesh with grid sizing at the wall and having a mesh with a cube-like shape provides greater accuracy. In terms of mesh refinement, an earlier study [2] used FEA to highlight that it is better to have more mesh elements along the stent struts' width rather than the struts' thickness due to the severe stress/strain variation across the strut's width. While these findings were consistent with other studies [19] [54], mesh convergence studies must be completed to verify the results as well as provide a balance between achieving an accurate solution and reducing the high computational cost.

2.3.3. Material

Material selection for coronary stents involves the consideration of visibility, mechanical integrity, radio-opacity and biocompatibility. Emphasising the significance of stent material development in commercial stents, one study [20] highlighted how stents made of stainless steel have largely been replaced with alloys including platinum chromium (PtCr) and cobalt-chromium (CoCr). These alloys provide greater strength and improved radio-opacity with less material resulting in thinner struts. Similarly, Ormiston et al. [17] showed that stents constructed of stainless steel were thicker and fractured more readily than those made with the cobalt alloys. Specifically, L-605 CoCr has been used in stent optimisation studies [2] as it has shown the least frequency of stent fracture when compared to first-generation stents, is biocompatible and has high mechanical strength.

2.3.4. Boundary Conditions

Compression Simulation

To test longitudinal compressive strength, the methodology behind experimental compression bench tests can be applied to FEA simulations. Ormiston et al. [55] performed compression bench tests on seven commercial stent designs using symmetrical loading. Using an Instron universal testing machine, the stents were compressed up to 5mm and the compressive force applied and stent shortening was recorded and plotted to compare stents' longitudinal strength. Similarly, one study [56] investigated the longitudinal stent deformation of five commercial stents through compression bench testing but also examined point loading in addition to symmetrical loading. The authors found that a greater range of clinical events could be simulated by analysing multiple compression lengths and loadings. While analysing results from point loading can provide a deeper investigation, the symmetrical compression loading condition has been used in the majority of studies as it determines the overall stent strength rather than at a specific location. The different loading conditions are illustrated in Figure 7. Applying this symmetrical loading to one side of the stent and fixing the other, an earlier study [57] was also able to produce a force-strain curve for 5 different commercial stent designs. This curve was used to determine each design's spring constant, yield force and ultimate strength. Moreover, the study was able to identify the point of permanent deformation and compressive stiffness for each design by incrementally increasing the vertical load.

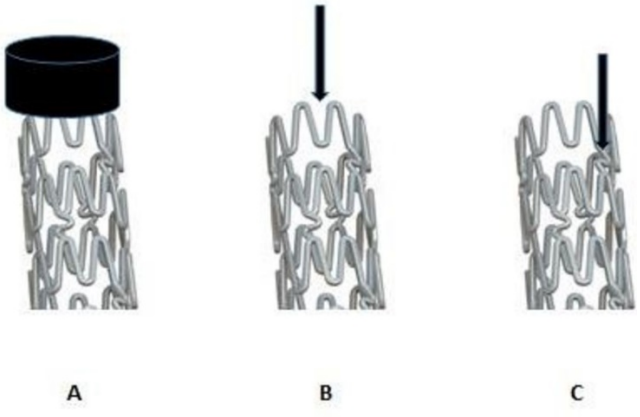

Figure 7. Compression Testing with Symmetrical Loading (A), and Point Loading (B & C) [56].

Bending Flexibility Simulation

To measure the bending flexibility of coronary stents, studies have measured deflection from three-point bending tests. This type of test was used by Wang et al. [53] and involves applying a downward load to the middle of the stent that is resting on two static support structures (Figure 8). This study specifically measured stent deformation and stress/strain distributions for each stent design, demonstrating that this test can investigate multiple outcomes including radial strength and flexibility. To analyse each stent's flexibility, a bending-force-deflection curve was generated from incrementally increasing the load and recording the reactive force and displacement of the loading applicator. A later study by the same author [58] demonstrated that this measured force and displacement could be used to derive the bending stiffness of the stent, which represents its flexibility. Therefore, the three-point bending tests can be used to determine, bending stiffness and the point of permanent deformation for stent designs.

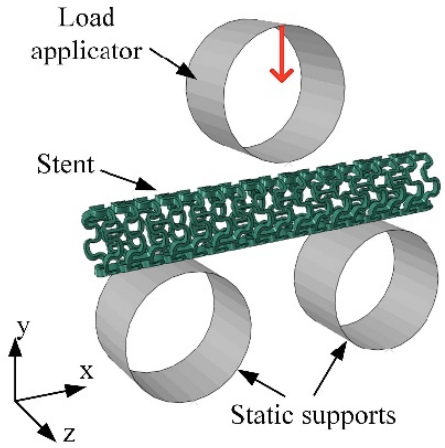

Figure 8. Three-Point Test Bending Set-Up [58].

Radial Strength Simulation

The radial strength of coronary stents is significantly analysed in literature due to the issue of elastic recoil. Kumar et al. [59] analysed the effect of stent design on various mechanical outcomes including radial strength, recoil and radial stiffness. The study simulated the expansion and crimping of the stent in five steps, mimicking the movements experienced by stents in their deployment and placement. In the final step of the simulation, a smoothly increasing pressure of 2 bar was applied to the external face of the stent, and the radial applied force and decrease in the stent's diameter was plotted for each design to identify each stent's radial strength. In a similar way, one study [60] recorded the radial force and diametric displacement of the examined stents through a simulation of crimping with a uniform radial displacement. The authors were able to determine the elastic radial stiffness of the stent from the gradient of the radial force to diametric displacement plot. Multiple other studies have similarly determined radial stiffness of stents based on the ratio of radial pressure or force to diametric displacement [61] [62]. Similarly, an earlier study [2] simulated radial strength testing by including an outer cylinder with a larger diameter than the stent in the simulation and progressively compressing the outer cylinder, subsequently compressing the stent to crimp (Figure 9). During the simulation, the solver recorded the radial-direction reaction force induced in the outer cylinder for each timestamp.

The maximum value of the total reaction forces was defined as the hoop strength and the stent radial strength could then be calculated by dividing this number by the length of the stent.

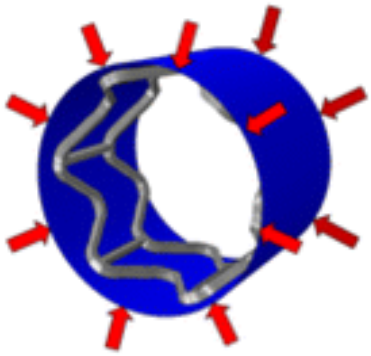

Figure 9. Radial Strength Stent Testing [63].

2.4. Computational Modelling of Coronary Flow with Computational Fluid Dynamics

Computational fluid dynamics (CFD) is a numerical method that can analyse and predict fluid flow behaviour that reflects real-life conditions. CFD has been used extensively in literature to optimise stent design by evaluating the haemodynamics of different designs, collecting detail and information that otherwise could not be measured from patient studies alone. While CFD can provide an accurate prediction of the behaviour of the blood flow, it has proven difficult to account for complete in vivo conditions including patient-specific geometry and lesions.

The mathematical process of CFD involves discretising a model into finite elements called mesh and then solving the governing Navier-Stokes equations for each element to provide a combined solution. The Navier-Stokes equations account for the conservation of mass, energy and momentum equations which are solved to predict flow characteristics including pressure and velocity [2]. The Navier-Stokes equation is defined as follows;

$$\rho \frac{\partial v}{\partial t} + \rho(v.\Delta)v = \mu_D \Delta^2 v - \Delta p + f \tag{5}$$

Where f is the body force, ρ is the fluid density, t is the time, v is the flow velocity, p is the pressure, μ_D is the dynamic viscosity and Δ is the divergence. When blood is assumed to be an incompressible fluid, this equation can be simplified further due to density being constant;

$$\Delta.v = 0 \tag{6}$$

While CFD can often provide an accurate representation of fluid flow, there are multiple limitations to CFD as a result of poor assumptions and over-simplification. Like FEA, complex geometries often require detailed mesh which results in a high computational cost, taking a significant amount of time to provide a converged solution. Hence, mesh sensitivity studies are completed to achieve accurate results while considering the computational cost. Despite the limitations of using CFD to model stented artery flow, it can provide predictions on the underlying flow behaviour and assist with stent design prior to prototype manufacturing in a cost-effective manner. The simplifications and decisions that have been made in regards to the stented model geometry, mesh structure, blood flow characteristics and boundary conditions, have been thoroughly investigated within literature.

2.4.1. Vessel Geometry

Plaque, vessel curvature and unsymmetrical vessel shape are patient-specific and difficult to simulate with CFD. One study specifically [64] investigated the effect of in-vivo conditions on stent geometry. Firstly, solid mechanics was used to model the expansion of a stent against simplified cylindrical arterial plaque, and then the deformed artery was subjected to fluid flow. This method is not common as it is thought that the inflation of the angioplasty balloon will primarily deform the artery. Typically, studies have opted for a simpler approach by modelling the arterial vessel as a cylinder with a constant diameter, and providing an imprint of the stent in this vessel with the Boolean operation in CFD [8] [11] [26] [37] [65]. Beier et al. [11] proposed that using idealised geometries has eliminated the local deformations caused by considering stent deployment and vessel curvature, enabling authors to focus on the underlying, primary aspects of stent design. The rigid-wall assumption has largely been used to simplify the model, and a comparison between fluid-structure modelling and CFD by one study [65] has validated this assumption is appropriate when studying WSS.

2.4.2. Meshing Structure

To numerically analyse the stented arterial model, it must be divided into finite volumes called mesh elements. Studies have carefully analysed and chosen mesh size, shape and the number of elements in order to provide accurate analysis. Unstructured tetrahedral meshes with defined mesh sizes have been commonly used for stent arterial modelling due to their simplicity and effectiveness in capturing rapidly changing features [11] [35] [64] [65]. These studies applied finer mesh to the stent imprint in the arterial wall due to its complexity and provided a courser mesh in the unstented region of the artery to save on the computational cost. To reduce the computational cost, mesh sensitivity studies are needed to determine the smallest number of mesh elements necessary to provide accurate results. While Pant et al. [8] determined the optimal number of mesh elements for each of the six designs investigated, another study [64] highlighted that parametric optimisation studies would expect a significant increase in the computational expense if mesh sensitivity studies were completed for each design.

2.4.3. Blood Characteristics

There has been debate in literature on whether blood should be considered Newtonian or non-Newtonian flow. One study [66] investigated two linear models and one nonlinear model when modelling blood flow through a stented artery, and determined that non-Newtonian models provide greater accuracy in their predictions of WSS. Specifically, modelling blood as a Newtonian fluid has led to the overestimation of restenosis risk by underestimating the WSS in stents. Newtonian models have been used in multiple studies for simplicity [8] [26] [65]. In this model, blood viscosity is assumed to be constant and of a magnitude found at high shear strain rates. However, this model provides great inaccuracy when measuring WSS as blood's viscosity changes with shear rate, and this rate varies from 0 to $1000s^{-1}$ over the cardiac cycle [67]. Moreover, the relationship between shear stress and strain is not linear. One study [68] compared multiple models that simulate artery blood flow and highlighted the effectiveness of the Carreau-Yasuda model in describing the shear-thinning, non-Newtonian behaviour of blood.

2.4.4. Boundary Conditions

Inlet Profile

Multiple studies modelling blood flow through stented arteries have specified the inlet flow to be laminar with a parabolic profile and for a no-slip condition to be applied to the wall [11] [64] [65] [66]. Importantly, studies have highlighted that the arterial vessel must be extended to provide additional inlet length and enable the flow to be fully developed at the stented arterial segment [11] [65]. Without the extra length, the flow will be uniform over the cross-section and will not reflect blood flow characteristics.

Pulsatile Flow

Pressure and velocity change rapidly in the cardiac cycle, and models have attempted to capture this by including pulsatile flow rather than steady flow in simulations. To reduce start-up effects on results and obtain a stable solution, multiple studies have analysed results taken from the fourth cardiac cycle [11] [64]. One study [66] specifically used 100 beats/min when modelling, using time-dependent boundary conditions. However, the significance of using pulsatile flow in stented artery models is disputed by one later study [26] that found a negligible difference between results from the steady inflow and pulsatile flow boundary conditions. It is likely that this result is from the error introduced from modelling the blood flow as Newtonian flow. Therefore, to accurately reflect the arterial haemodynamic environment, a time-dependent analysis, with pulsatile flow is preferred.

Outlet Profile

When modelling blood flow through a stented artery, it is largely agreed across literature that constant static pressure can be assumed at the outlet boundary [11] [64] [66]. To reduce the impact of the outlet cross-section border effects on the WSS results, studies have extended the arterial model at both ends, specifically by four diameters in length in one study [65]. Hence, studies have endorsed extending the artery model past the stented segment's outlet and assuming a constant static pressure at the outlet.

2.5. Motivation for Research

Overall, stent design has largely been influenced by the need to reduce mechanical failure and adverse effects on the haemodynamic environment in the preceding collective body of work. However, based on the review of literature, the consideration of all key design variables and their interdependent effects is a major collective shortfall. Whilst some studies investigated the optimisation of stents, only either haemodynamic or mechanical considerations were made and a limited number of variables were used. There are minimal studies that address stent design for both haemodynamic and mechanical outcomes concurrently, and those that do, individually assess four or fewer variables only. This major gap of knowledge presents a significant study opportunity and was thus the focus of this work whereby optimising stents based on the relationship between multiple design variables and multiple detailed objectives will assist in developing balanced and improved stent designs for commercial use.

Chapter 3 – Part 1: Methodology

3.1. Overview

Since the study aims to investigate the effect of different stent design variables on a stent's mechanical and haemodynamic performance and optimise stent design to benefit both areas, we generated an appropriate workflow. Figure 10 illustrates the overall process undertaken in this study which includes the development of the stent geometry with CAD, using the multi-objective optimisation process, and setting up the FEA and CFD simulations for each stent design.

There are two Parts to this study: Part 1 and Part 2. Part 1 was completed as originally proposed and is explained in Chapters 3, 4 and 5. Part 2 is explained in Chapter 6, and it outlines the substantial progress made towards a larger stent optimisation process that included more variables and objectives which paves the way for future work.

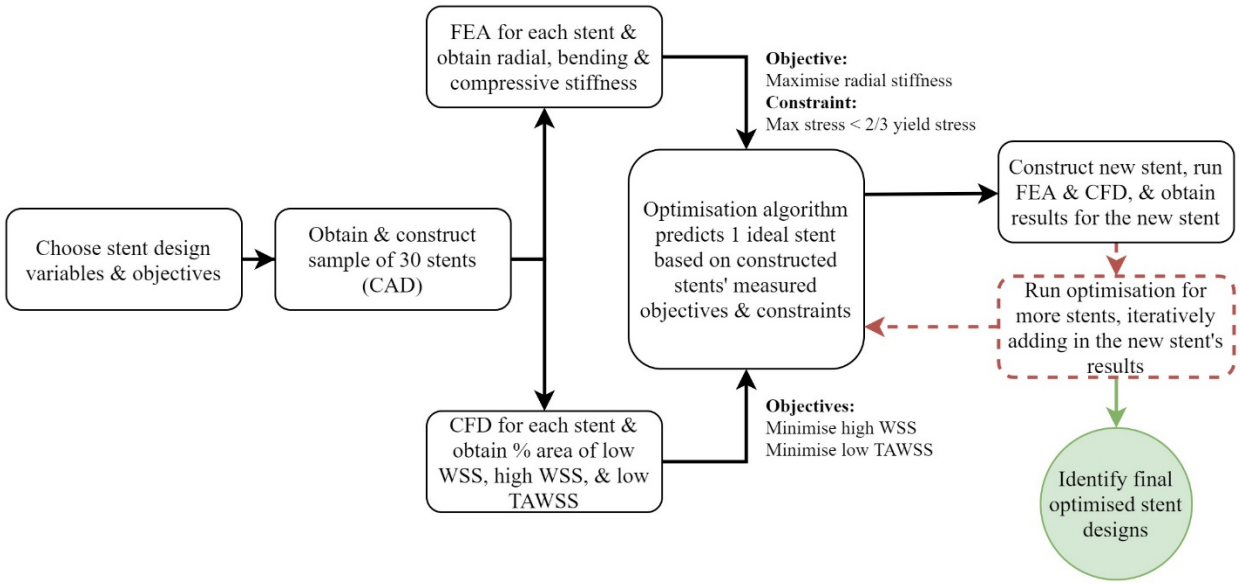

Figure 10. Methodology Overview Flowchart.

3.2. Stent Geometry

A computational model of each stent needed to be constructed in order to run the computational simulations. The stent geometry was efficiently created using a parameterised IronPython script that was developed in SpaceClaim API V18 ANSYS 19.2 Each stent was generated based on the design constraints and varied from the given design variables. When developing the script to construct the stents, consideration was made for both the eight significant design variables investigated in this study and the 10 total significant design variables that will be investigated in future work.

3.2.1. Design Variables

From reviewing key literature in stent design, each stent was constructed based on the key design variables illustrated in Figure 11 which includes the cross-sectional shape, strut thickness or diameter (SD1), strut width (SD2), intra-strut angle, alignment type, cell height, connector type, and the number of connectors.

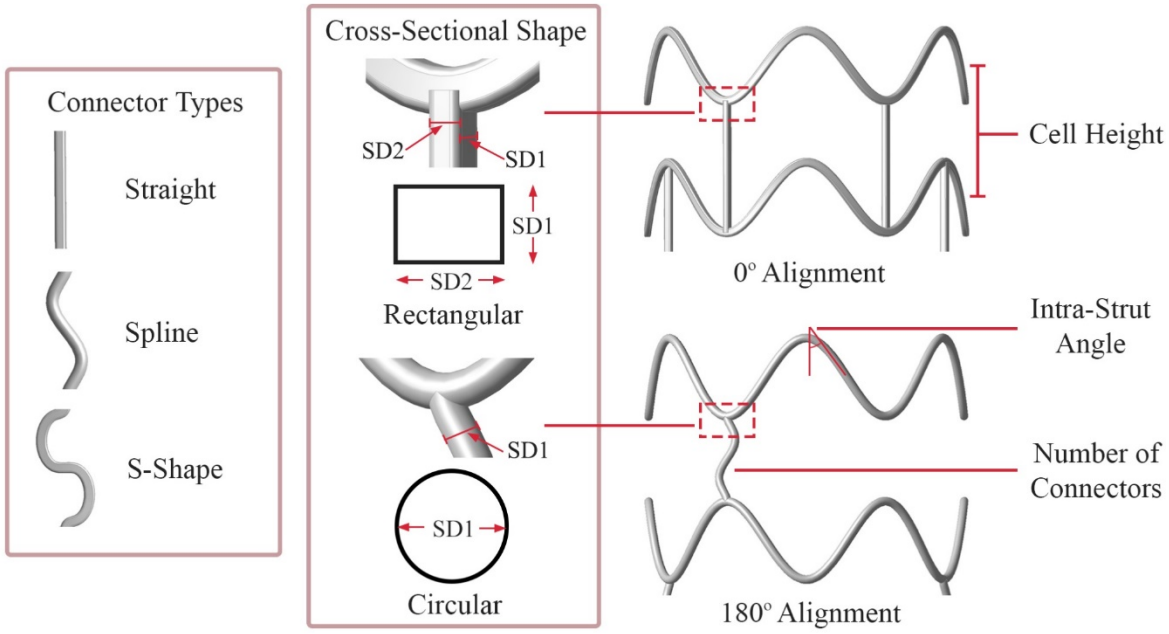

Figure 11. Stent Design Variables.

For stents with a rectangular cross-section, there were eight design variables, and for stents with a circular cross-section, there were seven design variables as 'Strut Dimension 2' did not apply. The specific design constraint ranges determined for each of the eight variables are given in Table 1.

Table 1. The Stent Design Variables and Constraint Range.

Design Variables	Design Constraint Range
Cross-Sectional Shape (CS)	Rectangular or Circular
Strut Dimension 1 (SD1, Strut Thickness or Diameter)	60 μm - 120 μm
Strut Dimension 2 (SD2, Strut Width)	60 μm - 120 μm
Intra-Strut Angle (SA)	25° - 50°
Alignment Type (AT)	0° or 180°
Cell Height (CH)	0.83 mm – 2.00 mm
Connector Type (CT)	Straight (1), Spline (2), or Semi-Circular (S-Shape) (3)
Number of Connectors (NC)	1 per cell (1), 2 per cell (2), alternating 1/2/1 (3)

The constraint range for each design variable was determined from key studies in stent design and based on the values used in the paper by H. Wright [69]. Specifically, the constraint range for the intra-strut angle considered the studies by Gundert et al. [34] [35], and the constraint range for the cell height reflects the study by Beier et al. [11]. The cross-sectional shape, strut dimensions, alignment and connector types have design constraint ranges that reflect what is commercially available. While the only stent with a circular cross-section is the Resolute Onyx (Medtronic), a circular cross-section was considered in addition to a rectangular cross-section due to the haemodynamic benefits shown by Poon et al. [27]. In addition, a chamfer of 15 μm was added to the edges of the rectangular struts to reflect more streamlined, commercial stents. The constraint range for the strut dimensions reflect the commercial designs discussed by Jiminez et al. [25] and the alignment and connector types of commercial stents are summarised well in studies such as the paper by Ormiston et al. [17]. For the stent generation script, parametrised equations were developed in 2D with DESMOS, an advanced online graphing calculator, to define each connector type as shown in Table 2.

Table 2. Connector Type Equations.

Connector	Equation
Straight	$f(z) = \{0 \le z \le 1 \quad : 0\}$
Spline	$f(z) = \{0 \le z \le 1 \quad : a_1 \cdot z^2(1-z)^2(0.5-z)\}$ $Where\ 0 < a_1 \le 30$
Semi-Circular (S-shaped)*	$f(z) = \begin{cases} 0 \le z \le b_1 - b_2 & : 0 \\ b_1 - b_2 \le z \le b_1 & : -\left(b_2^2 - \left(z - (b_1 - b_2)\right)^2\right)^{0.5} + b_2 \\ b_1 \le z \le 0.495 & : b_3 \cdot \left(\left(\frac{0.5 - b_1}{2} + 0.001\right)^2 - \left(z - \left(0.5 - \frac{0.5 - b_1}{2} + 0.001\right)\right)^2\right)^{0.5} + b_4 \\ 0.495 \le z \le 0.505 & : -b_5 \cdot z + b_5 \cdot 0.5 \\ 0.505 \le z \le 1 - b_1 & : -b_3 \cdot \left(\left(\frac{0.5 - b_1}{2} + 0.001\right)^2 - \left(z - \left(0.5 + \frac{0.5 - b_1}{2} + 0.001\right)\right)^2\right)^{0.5} - b_4 \\ 1 - b_1 \le z \le 1 - (b_1 - b_2) & : \left(b_2^2 - \left(z - \left(1 - (b_1 - b_2)\right)\right)^2\right)^{0.5} - b_2 \\ 1 - (b_1 - b_2) \le z \le 1 & : 0 \end{cases}$ $Where\ 0 < b_1 < 0.5, \quad 0 < b_2 \le 0.2, \quad 0 < b_3 \le 2, \quad 0 < b_4 \le 0.1, \quad 0 < b_5 \le 30$

* The Semi-Circular connector equation was complex as the script required the derivate of the function at the endpoints to be zero, and the connector shape needed to be able to adapt and fit a large range of stent designs and not protrude into the stent cell.

The constraint range for the number of connectors reflects commercial designs that have two connectors per cell, however, also considers a reduced number of connectors due to the haemodynamic benefits according to He et al. [22]. Based on the number of connectors, the connector arrangement was chosen so that the stent would be as stable as possible, taking alignment into consideration for the one connector per cell arrangement, and the patterns are illustrated in Figure 12.

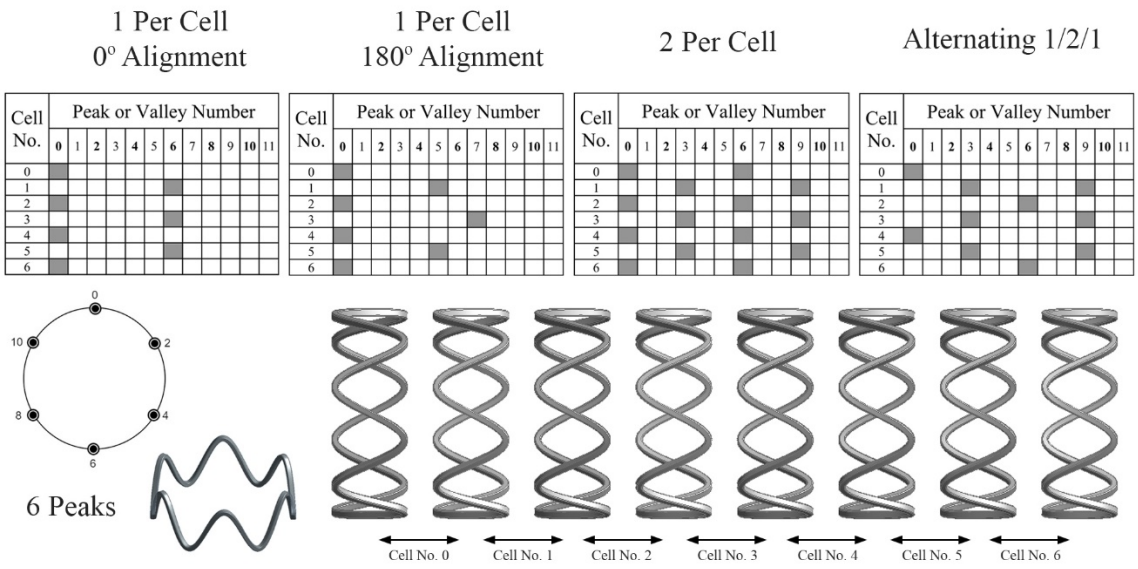

Figure 12. Connector Arrangement for 6 Peaks (Peaks are in Bold).

3.2.2. Design Constraints

Based on the literature review of stent design, an idealised, straight stent was considered suitable for this study, ensuring the focus was on the underlying aspects of stent design [11]. Considering what was commercially available, the stent diameter (D) was kept constant at 3mm, the stent's length was set to be a maximum of 12mm, and the number of peaks (NP) for each stent cell was six. Due to its high mechanical strength, biocompatibility and use in current commercial stents, L-605 cobalt-chromium was assigned as the material for the stents. Given the maximum length of the stent and the cell height (CH), the number of cells per stent was calculated as follows:

$$Number\ of\ Cells = ceil\left(\frac{11}{10 \times CH}\right)$$

Where 'ceil' is a function that rounds up the number to the nearest integer. Given the constant stent diameter, number of peaks and the intra-strut angle (SA), the amplitude of the stent cells was calculated as follows:

$$Amplitude = \frac{D \times \left(\frac{180}{NP}\right)}{4 \times \sin\left(90 - \frac{90}{NP}\right)\tan(SA)}$$

The stent design constraints are illustrated in Figure 13.

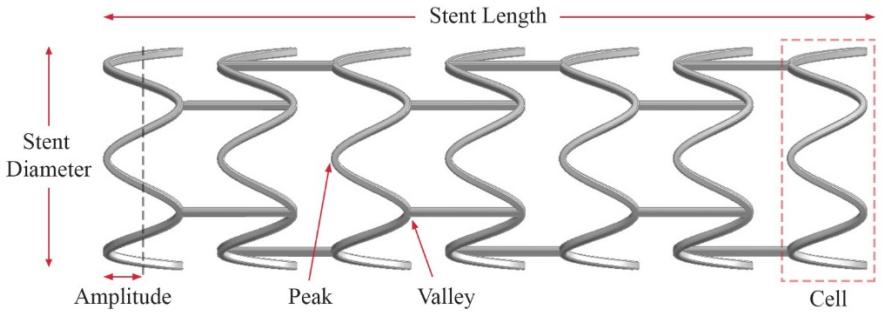

Figure 13. Stent Constraint Variables.

3.3. Multi-Objective Optimisation Process

The multi-objective optimisation process is outlined in Figure 14, and it aims to predict a set of stent designs with the best trade-off between competing objectives. The process starts by defining the design variables and their bounds (Section 3.2.1.). A sample of the stent designs based on these design variables was then obtained using Latin Hypercube Sampling. This method efficiently sampled the design space and a sample of 30 stent designs was generated for this study. This was deemed a reasonable number considering one additional solution would be sampled at each iteration (during the update process) and the overall budget was limited to 50 designs. The design variables were split in into three categories called discrete (CT, NC), continuous (SDA, SD2, SA, CH) and binary (CS, AT), and the design space was defined as follows;

$$CS = 1 \; or \; 2$$
$$60mm \leq SD1 \leq 120mm$$
$$60mm \leq SD1 \leq 120mm$$
$$25° \leq SA \leq 50$$
$$AT = 0° \; or \; 180°$$
$$0.83mm \leq CH \leq 2mm$$
$$CT = 1 \; or \; 2 \; or \; 3$$
$$NC = 1 \; or \; 2 \; or \; 3$$

After the 30 stents were generated using the script discussed in Section 3.2, the FEA simulations and CFD simulations were set up and solved for each stent as described in Sections 3.4 and 3.5 respectively. The results for each stent were recorded, and post-processed to identify values for the mechanical constraint and for the three objectives, two concerning the CFD simulation and one concerning the FEA simulation. The three objectives were defined as:

1. $Minimise\ the\ \%\ of\ Area\ with\ High\ WSS$
2. $Minimise\ the\ \%\ of\ Area\ with\ Low\ TAWSS$
3. $Maximise\ the\ Radial\ Stiffness$

When selecting the objectives, low TAWSS was selected over low WSS to consider the overall effect of low WSS on the vessel over the cardiac cycle rather than specifically at peak flow. Low WSS and low TAWSS are positively correlated, and hence the effect of high WSS was selected to be the other CFD objective. Radial stiffness was selected as the objective from FEA over bending and compressive stiffness, given in-stent restenosis is the greatest point of failure for stents and this predominantly occurs mechanically from a stent's elastic recoil. The mechanical constraint was defined as

$$Radial\ Maximum\ Stress \leq \frac{2}{3} \times Yield\ Stress$$

For the material considered in this study, L-605 cobalt-chromium, this meant that the maximum stress any stent could experience in both compression and tension was 333.33 MPa [70].

A surrogate modelling approach has been used by multiple stent design optimisation studies. This modelling approach involves the development of response surface models (RSMs) which predict the relationship between the design variables and objective functions. As a surrogate model is a regression system that can predict one objective or one constraint, each constraint and each objective will require its own surrogate model. The surrogate models in this study were constructed using Kriging (Gaussian Regression), which is used in the majority of stent optimisation studies [41], and each surrogate model constructed by Kriging is called a Krig. Hence, four Krigs were constructed for this study given the three objectives and one constraint.

Using the MATLAB optimisation code developed by Dr Ray Tapabrata, each Krig was initially constructed and trained based on the results obtained for the 30 initial stents. However, these initial Krigs are only a prediction and their accuracy required improvement before determining the optimum stent designs. The optimum stent designs were defined to be the set of non-dominated solutions, called the Pareto front, which are the designs that have at least one objective value that is better than another stent design. To improve the Krigs, an update process was required. The update process involved producing a new Latin Hypercube sample of 200 stent designs and then using the Krigs to predict what the results would be for these 200 designs. The optimisation algorithm called the non-dominated sorting genetic algorithm (NSGA-II) then searched the Krigs to create an initial Pareto front and used a fitness function called Expected Hypervolume Improvement (EHVI) to rank the 200 samples and iteratively change them to meet the objective goals. Based on the rank, the top stent design was constructed, its performance was simulated with the FEA and CFD simulations, and its results were added to the initial 30 stent results to update the Krigs. This update process was repeated for a total of seven new, updated stents as per the computational and time constraints.

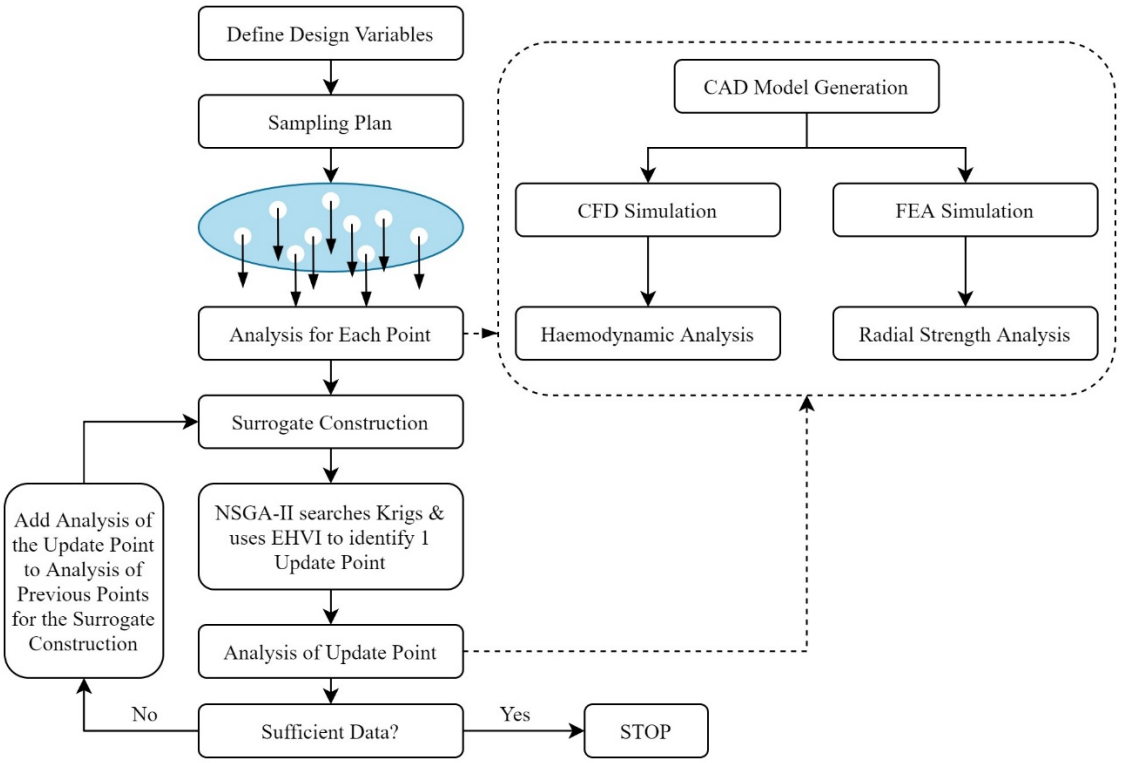

Figure 14. Multi-Objective Optimisation Process.

3.3.1. Sample of Stent Designs

The sample of 30 stents was constructed using the parameterised IronPython script as explained in Section 3.2 as illustrated in Figure 15. Of the 30 sample points, four stents (S03, S09, S12, S30) were unable to be created in CAD due to physical impossibilities including clashing cells, and a lack of room between cells for S-shape and spline connectors given the strut dimensions and cell height. These models were disregarded as they were outside of the feasible design space, and 26 sample points were used.

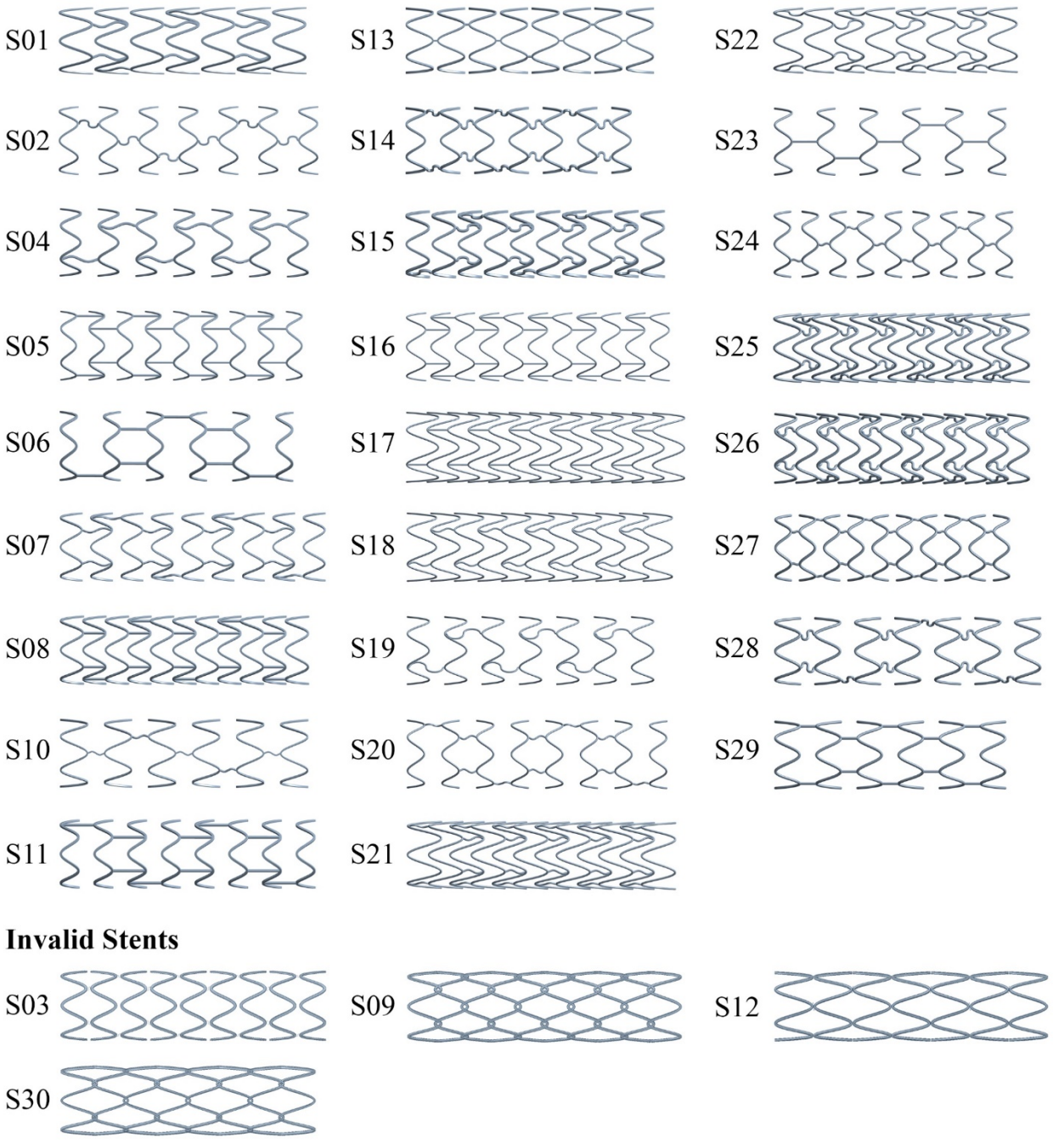

Figure 15. 26 Constructed Stents (Top) & Four Invalid Stents (Bottom).

3.4. FEA Modelling

When using FEA, the user is required to specify the geometry, mesh design, material and loading and boundary conditions. This geometry is then separated into elements called mesh that are each individually solved and together provide an approximate solution for the entire model. FEA was used in this study to imitate real-world environments with highly controlled conditions and investigate the mechanical strength of each stent in terms of its radial stiffness, bending stiffness, and compressive stiffness. Using the Static Structural module in ANSYS 19.2, these mechanical qualities were determined from three tests that were set-up based on the studies evaluated in Section 2.3.4; the radial strength simulation, bending flexibility simulation, and compressive strength simulation. For this study, only the radial stiffness of each stent was used as an objective in the process of optimisation. For future work, the bending stiffness and compressive stiffness of each stent will be used in the optimisation process to account for the flexibility and longitudinal strength of each stent.

For each of the three tests, it was determined that the stiffness needed to be calculated in the elastic region of the stress-strain curve to provide a consistent measure of stiffness that could be calculated from known equations that apply within the elastic region. To ensure that there were no outliers and that the results were recorded in the elastic region, three applied loads were used in each simulation test so that the average stiffness could be calculated for each stent. Two stents, S01 (rectangular cross-section) and S22 (circular cross-section), were used to test the simulation prior to its use in the optimisation process, and were able to determine three applied loads that would likely keep all of the stents in the elastic region. Once these three loads were determined for each of the three tests, the loads were parameterised in ANSYS 19.2 to provide an efficient process for retrieving the results after they had solved. To solve the FEA simulations, Katana, the UNSW shared computational cluster, was used.

3.4.1. Material

Design Modeler in ANSYS 19.2 needed to be used to create the additional geometry required for the FEA simulations' boundary conditions. As the CAD model stents were created in SpaceClaim in ANSYS 19.2, the stents were first exported as STEP files for circular strutted stents and as Parasolid Binary files for rectangular strutted stents to then be imported into Design Modeler. Once the stent model was imported successfully, the material could be assigned. The material assigned to the stents in all three tests of the current study was L-605 cobalt-chromium. Its material properties were sourced from stent design studies and are outlined in Table 3. L-605 cobalt-chromium was chosen as it is used in commercial stents such as the MULTI-LINK VISION (Abbott Vascular) stent [17] and the XIENCE Sierra stent (Abbott Vascular), and this material is known for its high mechanical strength and biocompatibility.

Table 3. Material Properties of L-605 Cobalt-Chromium

Material Properties	Value
Young's Modulus (MPa)	243 000 [70]
Poisson ratio	0.29 [71]
Density (kg/m^3)	9100 [70]
Tensile strength (MPa)	1000 [70]
Yield strength (MPa)	500 [70]

3.4.2. Boundary and Loading Conditions for the Radial Strength Simulation

The boundary and loading conditions for the radial strength simulation are illustrated in Figure 16 and were based on the set-up used in the study by Kumar et al. [59]. After previously testing the radial strength simulation with two stents (S01, S22) to determine the applied pressures that are likely within the stent's elastic region, a constant pressure of 0.02 MPa, 0.01 MPa, and 0.005 MPa were applied to the outside faces of each stent. For the boundary conditions, additional geometry was developed in Design Modeler. A cylinder was created to surround the entire stent and provide contact with the stent's outer surface. This contact was used to efficiently select all the outer faces of the stent when applying the external pressure. After the faces were selected, the cylinder was suppressed so it would not interfere with the simulation. For stents with a circular cross-section, an additional cylinder was created to slice the stent axially through its strut's centre providing an external face for the pressure to be applied. Each stent was sliced radially along the centre of each of its cells to create vertices for the boundary conditions. Using a cylindrical coordinate system, a fixed displacement in the angular and longitudinal direction was applied to the vertices of the stent along the centre of each of its cells. Once the simulation was solved for each of the applied pressures, the following values were recorded; the maximum Von Mises stress, the average total deformation, and the applied pressure surface area.

The results were post-processed to determine the radial stiffness for each stent. Based on multiple studies [60] [61] [62], the elastic radial stiffness can be determined from the ratio of the applied load to the diametric displacement of the stent. In this study, the radial stiffness was calculated for each of the three applied loads and averaged to ensure there were no outliers, and that the results were taken within the elastic region. The diametric displacement, applied force, and radial stiffness were calculated

$$\Delta D = D_1 - D_2 = 3mm - (3mm - 2 \times \delta) \tag{7}$$

$$F = P \times A_s \tag{8}$$

$$Radial\ Stiffness = \frac{F}{\Delta D} \tag{9}$$

Where ΔD is the diametric displacement, D_1 is the initial stent diameter, D_2 is the final stent diameter, δ is the average total deformation, F is the applied radial force, P is the applied pressure, and A_s is the applied pressure surface area.

The maximum Von Mises stress represented the maximum stress experienced by the stent during the radial strength simulation. The maximum stress value for the largest load (0.02 MPa) was constrained to be below 2/3 of the yield stress in the optimisation process, providing a factor of safety of 1.5.

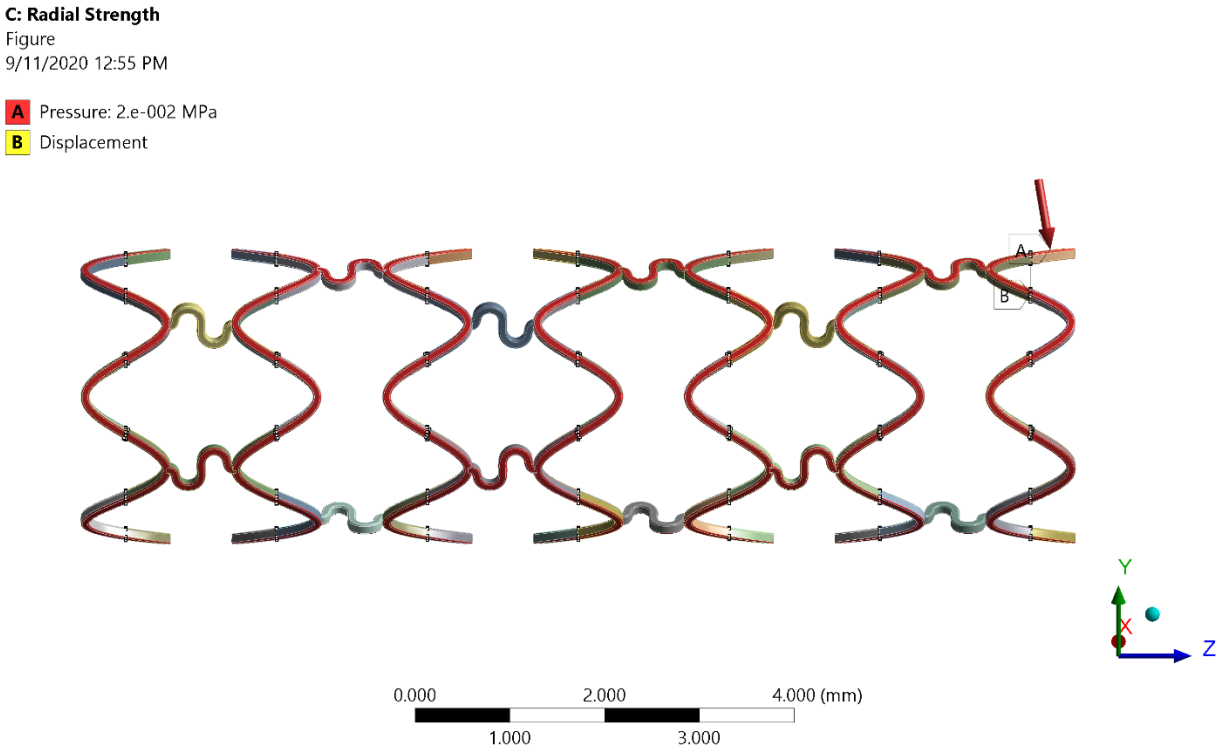

Figure 16. Boundary and Loading Conditions in ANSYS 19.2 for the Radial Simulation.

3.4.3. Boundary and Loading Conditions for the Bending Flexibility Simulation

The boundary and loading conditions for the bending flexibility simulation are illustrated in Figure 17. This simulation was previously validated by A. Senthurnathan [72] where the setup was based on the study by Wang et al. [58]. After previously testing the bending flexibility simulation with two stents (S01, S22) to determine the applied loads that are likely within the stent's elastic region, a constant force of 0.01 N, 0.005 N, and 0.001 N in the x-direction was applied to the centre cell for stents with an odd number of cells, or to the two centre cells for stents with an even number of cells. For the boundary conditions, additional geometry was developed in Design Modeler. Two structural steel cylinders, with an arbitrary external diameter of 5.1mm and a wall thickness of 1.1mm, were placed at the centre-line of the end cells on each side of each stent. The contact between the stent and the two cylinders was set to be bonded. A fixed support and cylindrical support boundary condition were applied to the outer face of the two cylinders. Once the simulation was solved for each of the applied forces, the following values were recorded; the maximum Von Mises stress, and the minimum directional deformation in the direction that the force was applied (x-direction).

The results were post-processed to determine the bending stiffness for each stent. Based on the study by Wang et al. [58] and previously validated by A. Senthurnathan [72], the elastic bending stiffness can be determined through the bending theory, whereby there is a three-point bending system and the loads are within the material's elastic limit. In this study, the bending stiffness was calculated for each of the three applied loads and averaged to ensure there were no outliers, and that the results were taken within the elastic region. The active length (distance between the cylinders), and bending stiffness were calculated

$$l = ceil\left(\frac{11}{CH}\right) \times CH - CH \tag{10}$$

$$Bending\ Siffness = \frac{Fl^3}{48\delta} \tag{11}$$

Where F is the applied force, l is the active length, and δ is the maximum deflection (the minimum directional deformation).

The maximum Von Mises stress represented the maximum stress experienced by the stent during the bending flexibility simulation. In future work, the maximum stress value for the largest load (0.01 N), will be constrained to be below 2/3 of the yield stress in the optimisation process, providing a factor of safety of 1.5.

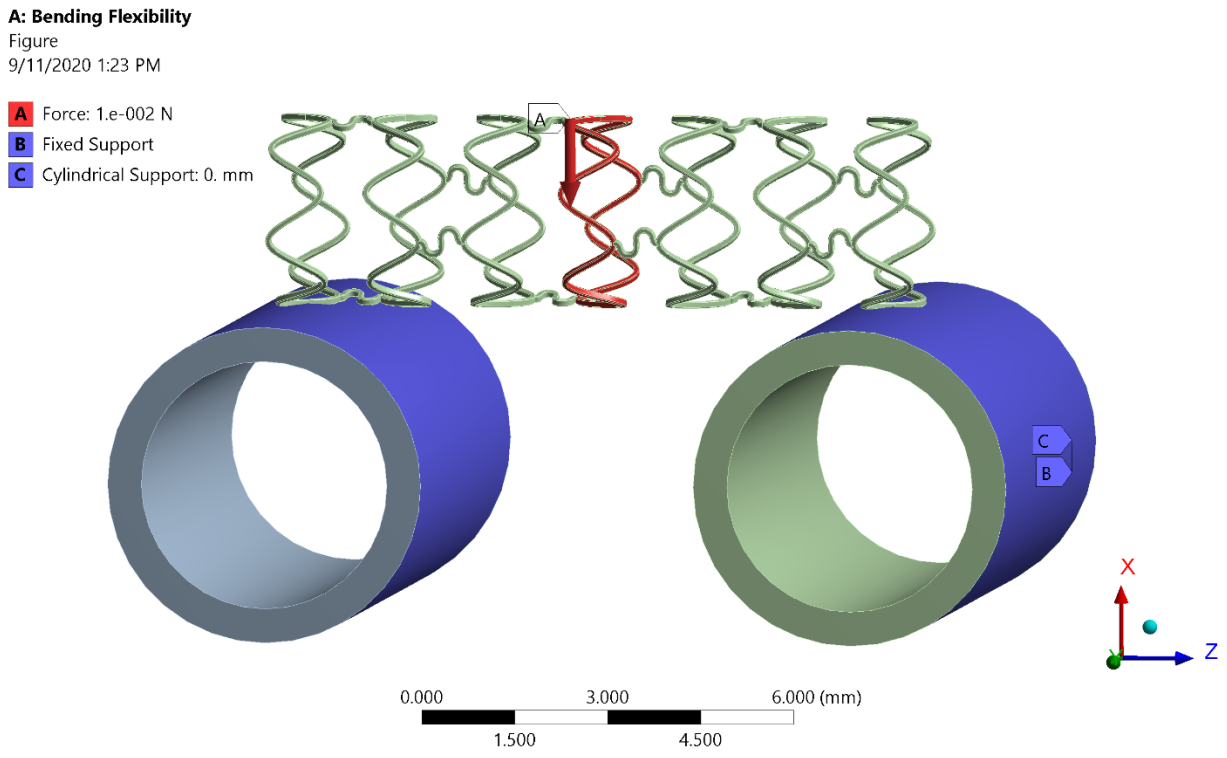

Figure 17. Boundary and Loading Conditions in ANSYS 19.2 for the Bending Simulation.

3.4.4. Boundary and Loading Conditions for the Compressive Strength Simulation

The boundary and loading conditions for the compressive strength simulation are illustrated in Figure 18. This simulation was previously validated by A. Senthurnathan [72] where the setup was based on the study by Ormiston et al. [55]. After previously testing the bending flexibility simulation with two stents from the sample of 30 (S01, S22) to determine the applied loads that are likely within the stent's elastic region, a constant force of 0.004 N, 0.002 N, and 0.001 N in the z-direction was applied to the stent cell on one end of the stent. A fixed support was applied to the stent cell on the opposite end of the stent. Once the simulation was solved for each of the applied forces, the following values were recorded; the maximum Von Mises stress, and the maximum directional deformation in the direction that the force was applied (z-direction).

The results were post-processed to determine the compressive stiffness for each stent. Previously validated by A. Senthurnathan [72], the elastic compressive stiffness can be determined through Hooke's Law within the linear elastic limit of the material. In this study, the compressive stiffness was calculated for each of the three applied loads and averaged to ensure there were no outliers, and that the results were taken within the elastic region. The compressive stiffness was calculated

$$Compressive\ Stiffness = \frac{F}{\delta} \tag{12}$$

Where F is the applied force, and δ is the compressed distance of the stent (the maximum directional deformation).

The maximum Von Mises stress represented the maximum stress experienced by the stent during the compressive strength simulation. In future work, the maximum stress value for the largest load (0.004 N), will be constrained to be below 2/3 of the yield stress in the optimisation process, providing a factor of safety of 1.5.

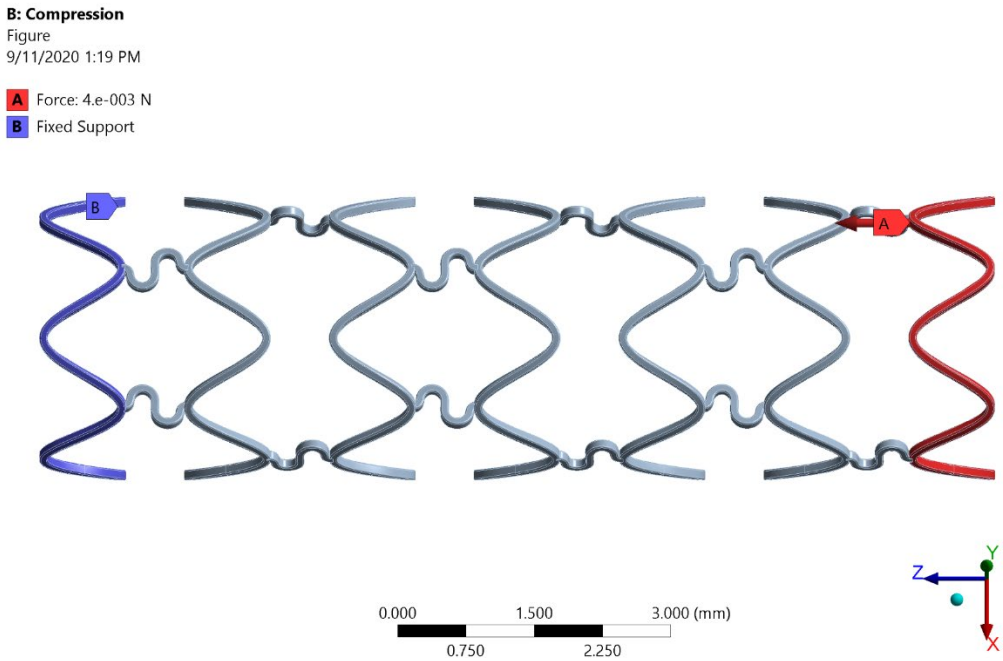

Figure 18. Boundary and Loading Conditions in ANSYS 19.2 for the Compression Simulation.

3.4.5. Mesh Generation and Sensitivity

Based on the review of stent design literature, the stent models for all three simulations were meshed with an unstructured, patch-conforming tetrahedron mesh, and the stent's body mesh element size was refined (illustrated in Figure 19). The previous mesh sensitivity study in the paper by A. Senthurnathan [72] verified the simulations based on two stent models, a stent with a circular cross-section, and a stent with a rectangular cross-section, and determined that at least 200, 000 mesh elements and at least 300, 000 mesh elements provided accurate results for the compressive strength simulation and bending flexibility simulation respectively. In the interest of reducing computational time, a coarse mesh was applied to the support cylinders in the bending flexibility simulation as there was no analysis being conducted on these models.

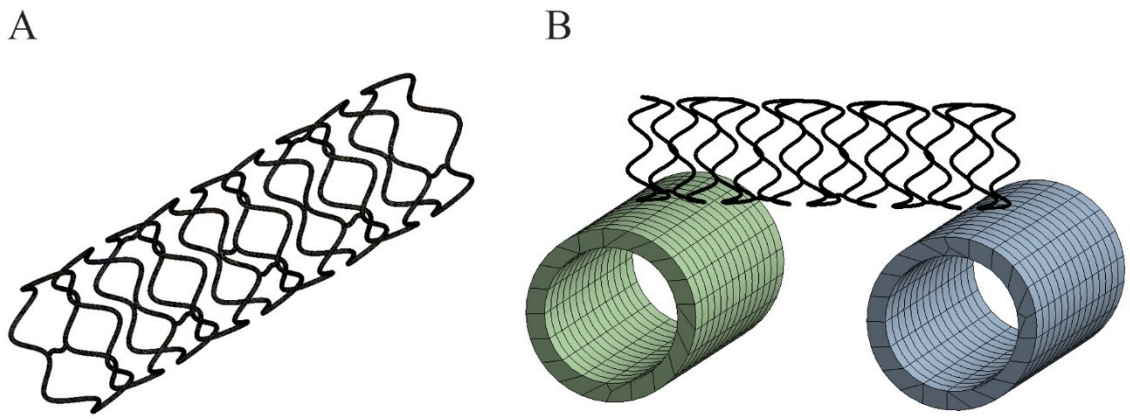

Figure 19. Mesh for the Compressive and Radial Strength (A) and Bending Simulations (B).

For verification of the radial strength simulation, a mesh sensitivity study was completed in this study and is illustrated in Figure 20. Two stents from the sample of 30 stent designs were used in the mesh sensitivity study; S06 which has a rectangular cross-section and straight connectors, and S24 which has a circular cross-section and spline connectors. Testing for both cross-sections with different connector types ensured that the mesh refinement was suitable for both cross-section types, which have a slightly different set-up process for the radial simulation. Similar to the compressive strength simulation, it was determined that at least 200, 000 mesh elements for the radial strength simulation would produce accurate results as this is where results begin to converge. This provided a balance between high computational cost and accurate solutions for the radial strength simulation. As indicated in Figure 20, a body element mesh size of 0.032mm was found to achieve at least 200, 000 mesh elements for the stents tested in this study.

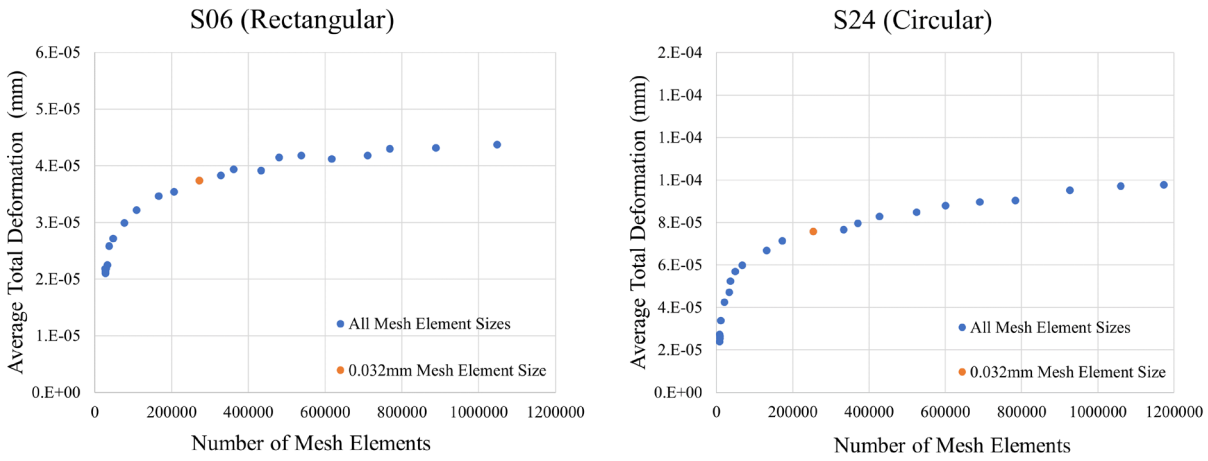

Figure 20. Mesh Sensitivity Study for the Radial Strength Simulation.

3.4.6. Validation for the Radial Strength Simulation

To ensure the results produced from the radial strength simulation were valuable and accurately represented real-life conditions, the radial strength simulation was validated using the study by Kumar et al. [59]. The paper by A. Senthurnathan [72] had used this study to validate the results from analysing a single stent cell, however, the radial strength setup needed to be expanded to incorporate the entire stent to account for the effect of the other design variables such as the connector type and the cell height. A computational model of the stent cell from the study by Kumar et al. was recreated to be as close as possible to how it was described in the study, and an entire stent was also created using this stent cell design, 2 straight connectors per cell, and a cell height of 1.9805mm. The created models are pictured in Figure 21.

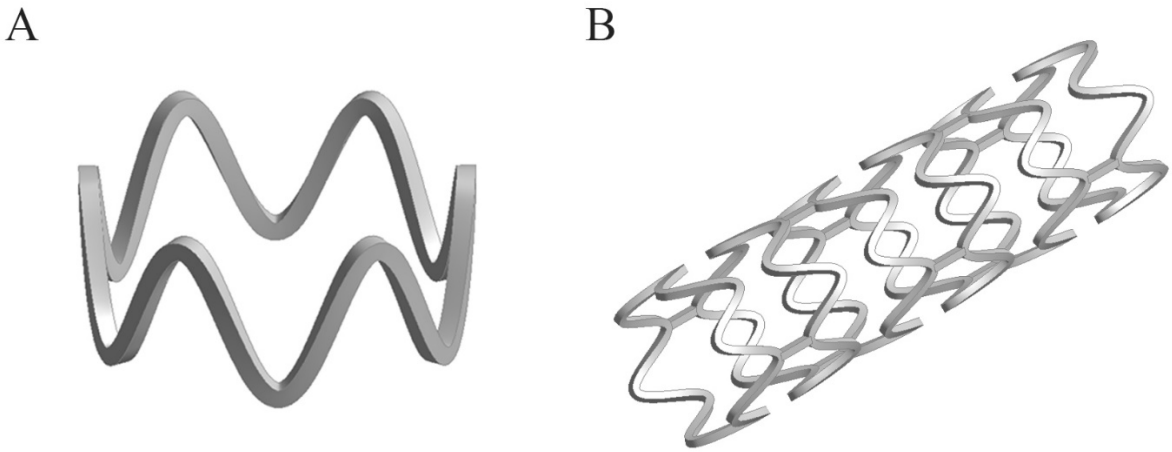

Figure 21. The Recreated Cell (A), & Entire Stent (B) for the Validation Study.

Using ANSYS 19.2 and assigning the material PLLA to the stents, the boundary and loading conditions that were applied to the single cell were applied to the entire stent. The results recorded for both the single cell and the entire stent were compared to the results from the study by Kumar et al. in a radial force to stent diameter plot illustrated in Figure 22 which identifies that the current study produces results that are very similar to the literature results in the elastic region. The difference between the literature and recreated cell results are likely from the stent cell geometry being slightly different from the model used in the study. The radial stiffness has been known to be more attributed to a unit stent cell's properties, while the compressive and bending stiffness are more attributed to the connectors [59]. This explains why the stent cell and the entire stent model produced similar results in this validation study. Hence, the radial strength simulation is suitable for evaluating the elastic radial stiffness of an entire stent model.

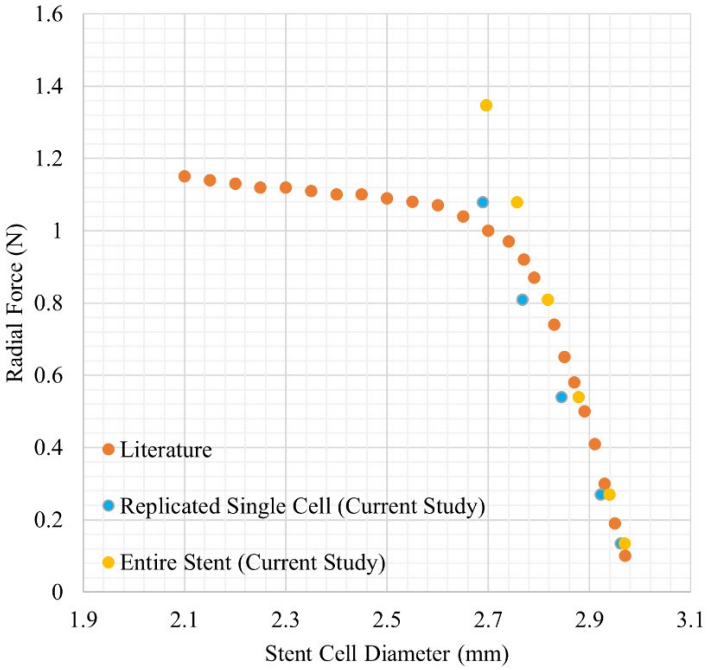

Figure 22. Radial Strength Simulation Validation Study [59].

3.5. CFD Modelling

CFD was used in this study to predict the blood flow behaviour exhibited for each stent in a stented artery, imitating real-life conditions in a controlled environment. Like FEA, the user is required to specify the geometry, mesh design, material and loading and boundary conditions for CFD simulations. The model is discretised into mesh elements and the governing Navier-Stokes equations are solved for each of these elements to provide a combined approximate solution for the entire model. Using the CFX module in ANSYS 2019 R3, the CFD simulations in this study were set-up to investigate the WSS and TAWSS induced in the stented region of the artery during the cardiac cycle. While the percentage of area with low WSS was recorded in this study, only the percentage of area with high WSS and low TAWSS were used as objectives in the optimisation process of this study. The CFD simulation set-up was developed by H. Wright [69], and is a largely automated process. Katana, the UNSW shared computational cluster was used to solve the CFD simulations.

3.5.1. Arterial Vessel Modelling

Using Design Modeler in ANSYS 2019 R3, the arterial environment was simulated by generating a cylinder 3mm in diameter and using the Boolean subtraction operation to cut into the cylinder with the imported stent model at 50% protrusion (illustrated in Figure 23). The cylinder was constructed to be 43mm in length as it was designed to include an outlet length of 4mm and an inlet length of at least 27mm, given the stent was at its maximum length of 12mm. The outlet length was chosen arbitrarily but was done to account for any downstream disturbance. Based on the inlet flow conditions explained in Section 3.5.3 and to ensure fully developed flow in the stent segment, the inlet length was calculated based on the vessel diameter, and Reynolds number of 150, and determined from the following formula [11];

$$Inlet\ Length = 0.06 \times Re \times Vessel\ Diameter \tag{13}$$

Where Re is the Reynolds number.

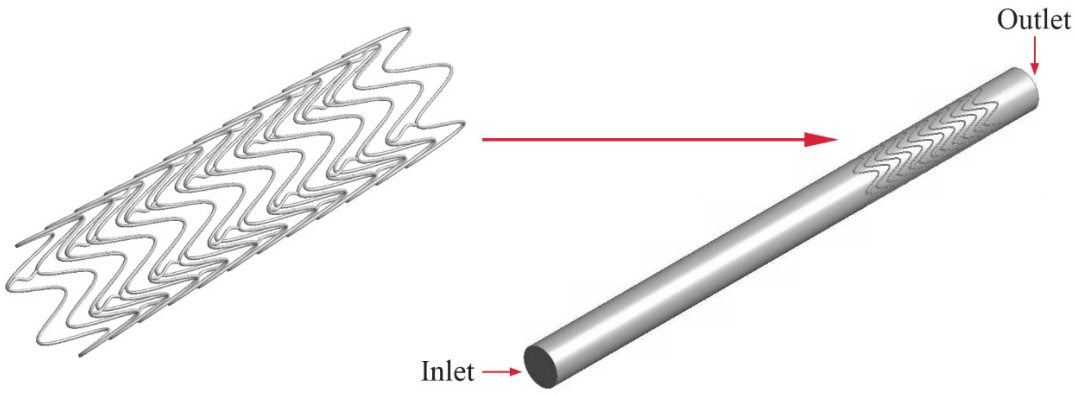

Figure 23. CFD Geometry Construction.

3.5.2. Mesh Generation and Sensitivity

The entire stented vessel was meshed with a patch-conforming tetrahedron mesh, that was refined at the vessel's outer wall with an inflation layer, and a finer mesh was applied to the stent imprint (illustrated in Figure 24). This meshing approach was adopted as it was seen to be successful in multiple other studies [11] [35] [64] [65]. To refine the mesh, an inflation layer was applied to the vessel's outer wall as this was where the WSS results were to be taken from, given that the imprint of the stent is along the vessels outer wall. A mesh size of 0.13mm ensured that the unstented region of the vessel contained coarser mesh to save on computational cost. Due to the complexity of the stented region, a finer mesh was applied to this region by applying an element size factor of 0.008. To determine the mesh elements required to produce accurate solutions within a reasonable computational load, a mesh sensitivity study was previously completed, however, was not performed for every stent model due to time and computational constraints. The mesh sensitivity study determined that an average of 10 million elements would be required per model, however, the number of mesh elements was dependent on the stent geometry, and the number of required elements increased to 25 million elements for complex stent geometries such as those with S-shape connectors.

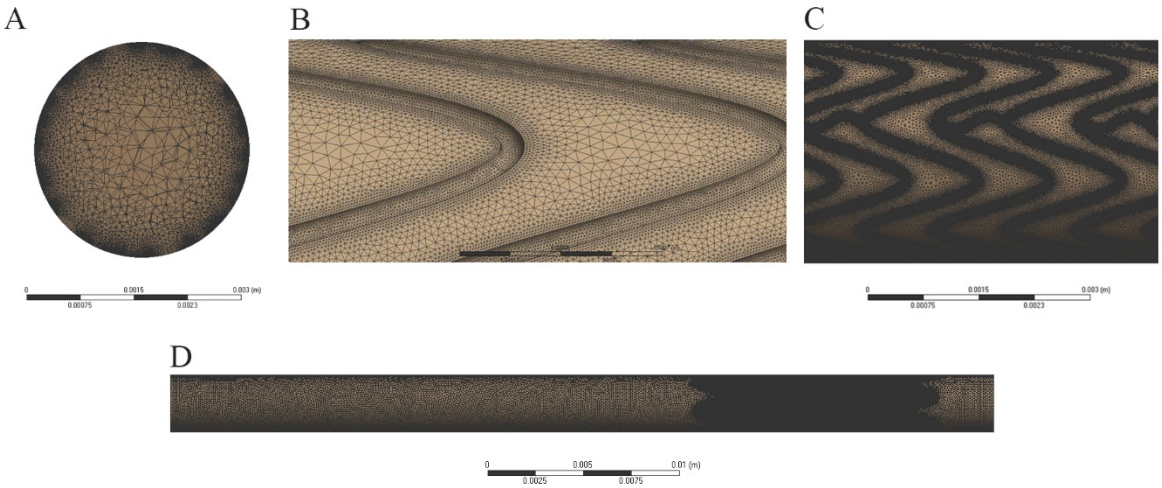

Figure 24. Stented Segment Cross-Section (A), Stent Imprint (B, C), and Entire Vessel Mesh.

3.5.3. CFD Environment

Using CFX in ANSYS 2019 R3, the boundary conditions, vessel and fluid properties, and transient settings were defined with respect to the studies by Pant et al. [8] and Beier et al. [11]. Adapting the method from Beier et al., each CFD simulation was run until the solution converged with a residual errors target of 10^{-4}.

Boundary Conditions

At the inlet, a parabolic flow was defined based on the following equation;

$$U = v_{max}\left(1 - \frac{r^2}{r_{max}^2}\right) \tag{14}$$

Where r_{max} is the radius of the vessel, r is the distance from r_{max} to the centre line, and v_{max} is the velocity at the vessel's centreline.

To imitate the pulsatile flow, a flow rate versus time of 0-129 mL/min was applied to the vessel's inlet. This value was adapted from Pant et al., where an average velocity of 0.1629 m/s is applied. The equation used to determine the maximum flow rate is as follows;

$$Inflow\ rate = v_{average} \times A_1 \times 1.8667 \tag{15}$$

Where $v_{average}$ is the average velocity, A_1 is inlet area, and 1.8667 is the scaling factor that was applied because the flowrate in this study was measured at the peak flow rather than the average flow.

A no-slip wall condition was applied to all the internal surfaces. At the outlet, a spatially and time constant static pressure was prescribed.

Vessel and Fluid Model Properties

Based on previous studies, the vessel was simplified to be rigid and without motion, reducing the computational cost. The vessel was modelled as blood with a density of 1060kg/m^3 [11] and a laminar fluid model was used since blood flow has been assumed laminar in multiple studies. The Carreau-Yasuda model was used to account for the non-Newtonian behaviour of blood and is defined by Razavi et al. [68] as follows;

$$\mu_a = \mu_\infty + \left(\frac{\mu_0 - \mu_\infty}{(1 + (\lambda\dot{\gamma})^a)^{\frac{1-n}{a}}} \right) \tag{16}$$

Where μ_a is the apparent viscosity, μ_0 is the constant viscosity, μ_∞ is the high shear viscosity, λ is a time constant, $\dot{\gamma}$ is the shear strain rate, n is the index, and a is the Yasuda exponent.

Transient Settings

Following a steady-state analysis, four consecutive cycles were simulated to reflect the cardiac cycle. From the time step convergence study, a time step of 0.005s was selected for the transient solution, and the Second Order Backward Euler with High-Resolution advections scheme was used. The CFD simulation was separated into three stages; Steady-State, Transient 1 and Transient 2. The first stage found the solution for a steady-state analysis and this solution was used to begin the Transient 1 set-up which simulated the first three cycles. Finally, the Transient 2 set-up simulated the fourth cycle. With each cycle taking 0.72 seconds, a total of 144 time steps were required per cycle based on the time step. Table 4 shows the time simulated for the Transient 1 and Transient 2 simulations.

Table 4. Transient Solution Temporal Set-up.

	Initial Time (s)	**Total Time (s)**
Transient 1	0	2.16
Transient 2	2.16	2.88

To obtain a stable solution and reduce start-up effects, the results were taken from the fourth cardiac cycle [11]. Figure 25 is the blood flow waveform over time by Nichols et al. [67] that has been vertically scaled by H. Wright [69] to have the same average flow rate as Pant et al., and is the prescribed inlet boundary condition in this study. The percentage of area with low WSS (WSS < 1 Pa [14]) and high WSS (WSS > 3 Pa [16]), as defined in Section 1.2.1, were measured at peak flow which is the second last time step indicated in Figure 25 at 2.72s. As the TAWSS averages the WSS over time, the percentage of area with low TAWSS (TAWSS < 1 Pa [14]) was measured from the last time step at 2.88s.

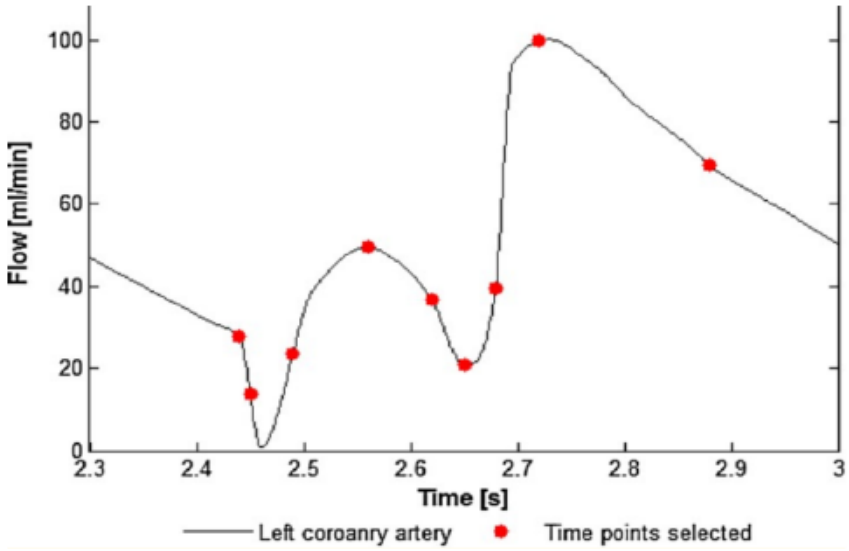

Figure 25. Blood Flow in the Left Main Coronary over Time (adapted from Nichols et al.) [69].

Chapter 4 - Results

4.1. Initial Sample Performance

To analyse the haemodynamic and mechanical performance of each stent in the initial sample of 30 stents, the results obtained from the CFD and FEA simulations were recorded in Table 5. This included the percentage of area with low WSS (LWSS), with high WSS (HWSS), and with low TAWSS, as well as the radial stiffness, bending stiffness, compressive stiffness (Comp Stiffness) and maximum stress recorded for each simulation at the highest applied load. Analysis of the initial Latin Hypercube sample of 30 stents determined that there were 17 non-dominated (ND) solutions, five with a rectangular cross-section, and 12 with a circular cross-section. A non-dominated solution is a solution that has at least one objective value that is better than another stent design.

In Table 5, * marks an ND solution, ** marks a solution that was no longer an ND solution after the update process, ^ marks an objective or constraint that was used in the multi-objective process, R refers to a rectangular cross-section, and C refers to a circular cross-section. The remaining variables are explained in Table 1 of Section 3.2.1. The results for stress were based on the maximum loads applied which were 0.02MPa, 0.01N and 0.0004N for the radial, bending and compression simulations respectively. In addition, 'Inf" has been used to represent the result for the 4 invalid stent designs.

Table 5. Initial Sample Performance.

#	CS	SD1 (μm)	SD2 (μm)	SA (°)	AT (°)	CH (mm)	CT	NC	LWSS (% Area)	HWSS (% Area)^	TAWSS (% Area)^	Radial Stiffness (N/mm)^	Bending Stiffness (Nmm^2)	Comp Stiffness (N/mm)	Radial Stress (MPa)^	Bending Stress (MPa)	Comp Stress (MPa)
01	R	61	109	27.917	0	1.6295	2	3	2.7671	83.6521	7.8444	900.24	0.65430	0.01554	92.757	260.380	127.035
02	R	63	81	43.750	180	1.7855	3	1	3.3671	84.2331	6.8145	857.08	0.52897	0.00787	76.554	459.301	159.465
03	R	69	115	36.250	180	1.3175	3	2	Inf	Inf	Inf	Inf	Inf	Inf	Inf	Inf	Inf
04*	R	75	101	41.250	0	1.7075	2	1	4.0714	80.3333	8.3884	1623.57	1.02186	0.01667	48.252	320.266	114.952
05*	R	77	61	49.583	0	1.2395	1	2	4.3356	79.7601	8.7267	2229.67	2.14732	0.13987	47.113	155.446	27.440
06*	R	81	113	48.750	180	1.9025	1	3	3.6780	82.9908	7.4111	3063.51	2.60554	0.05328	42.159	87.290	63.963
07	R	85	65	39.583	0	1.3565	2	3	6.1222	71.5840	12.3468	880.82	0.64210	0.01616	84.318	263.359	112.860
08*	R	89	83	37.917	0	1.0055	1	3	7.8165	61.0780	15.6353	1947.62	0.89465	0.02249	82.482	193.223	85.738
09	R	91	99	28.750	180	1.1615	2	2	Inf	Inf	Inf	Inf	Inf	Inf	Inf	Inf	Inf
10	R	93	67	32.917	180	1.9805	2	1	4.5972	78.5465	9.3762	449.23	0.54795	0.01613	100.364	167.776	90.006
11**	R	97	105	44.583	0	1.5125	1	3	6.1044	71.1934	12.2786	3111.67	3.34949	0.05562	58.301	218.239	55.613
12	R	101	91	25.417	180	1.7465	3	1	Inf	Inf	Inf	Inf	Inf	Inf	Inf	Inf	Inf
13	R	103	75	32.083	180	1.4735	1	1	7.2654	70.5565	14.1878	830.72	0.72901	0.02090	111.729	167.461	76.049
14	R	109	89	42.083	180	1.5905	3	2	7.0723	70.9690	13.2889	1351.31	8.15779	0.50898	74.506	62.778	10.703
15	R	115	95	37.083	0	1.2005	3	3	9.9320	54.4549	19.4648	2193.99	1.94723	0.04857	79.695	150.510	54.516
16*	C	65	-	42.917	0	1.0835	1	2	2.6083	77.0209	8.4302	1003.06	0.90801	0.04546	141.899	327.751	50.070
17*	C	67	-	29.583	0	0.8885	1	1	3.4953	66.7449	11.2485	545.13	0.17630	0.00227	239.959	544.710	207.831
18*	C	71	-	31.250	0	1.0445	2	1	3.3932	72.2530	9.9722	567.83	0.16293	0.00333	218.456	586.109	187.278
19*	C	73	-	38.750	0	1.6685	3	1	1.1337	86.4426	6.1870	488.69	0.32191	0.00584	157.567	439.507	187.735
20*	C	79	-	46.250	180	1.5515	2	3	2.8564	81.1688	7.3228	1160.79	0.93232	0.01612	110.292	404.696	136.484
21	C	83	-	27.083	0	0.9665	2	2	4.9616	57.5091	13.9864	936.99	2.06919	0.08273	355.943	119.443	24.412
22*	C	87	-	30.417	0	1.4345	3	2	3.6248	73.4336	9.8055	890.55	3.29769	0.16149	215.882	96.494	20.594
23*	C	95	-	45.417	180	1.9415	1	1	2.6056	83.5006	6.4855	1414.99	1.02063	0.02222	97.985	120.764	73.404
24*	C	99	-	47.083	180	1.2785	2	1	4.2400	72.4780	10.0965	2631.19	1.10762	0.02130	82.825	159.116	71.822
25*	C	105	-	33.750	0	0.8495	3	3	7.5578	51.6683	17.8747	2318.51	2.43990	0.02829	177.730	103.767	67.752
26*	C	107	-	40.417	0	0.9275	3	2	7.1974	54.1819	16.7614	3961.70	7.29195	0.29951	106.552	75.043	10.912
27*	C	111	-	47.917	180	1.1225	2	2	5.5396	67.6140	12.8742	5421.89	16.64332	0.52164	80.646	59.327	9.384
28	C	113	-	34.583	180	1.8245	3	3	4.4843	72.9178	10.4242	1238.04	2.54557	0.04920	175.287	108.874	50.933
29*	C	117	-	35.417	180	1.8635	1	2	3.4333	76.9466	8.4996	1664.01	26.45488	0.89240	177.249	47.224	8.969
30	C	119	-	26.250	180	1.3955	1	3	Inf	Inf	Inf	Inf	Inf	Inf	Inf	Inf	Inf

The 17 non-dominated solutions from the initial sample are illustrated in Figure 26. A trade-off between high WSS and low TAWSS was identified. The sparseness of non-dominated solutions for higher values of radial stiffness suggested that there needed to be development of the stent designs to maximise radial stiffness.

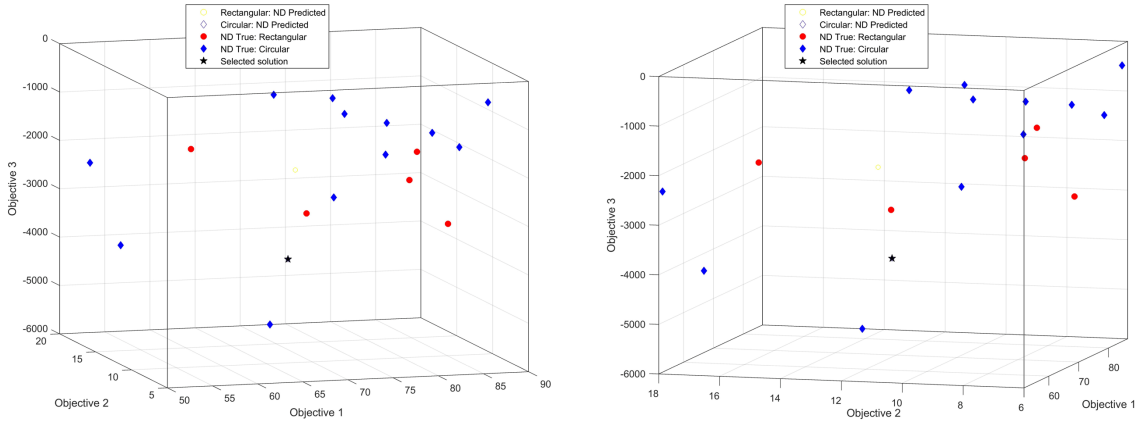

Figure 26. Comparison of Objective 1 (Minimising High WSS), Objective 2 (Minimising Low TAWSS), and Objective 3 (Maximising Radial Stiffness) for the Initial Non-Dominated Solutions.

4.2. Updated Stent Designs

As discussed in Section 3.3, the surrogate models (Krigs) were searched using NSGA-II, ranked with EHVI to identify one update stent design, and then updated with the results from the new designs. The seven updated stent designs from the multi-objective optimisation process are illustrated in Figure 27. All the updated designs had a circular cross-section with two connectors per cell, and six out of the seven design points had spline connectors and an alignment of 180 degrees. Notably, all of the updated designs had thicker strut dimensions (> 99.5 um) and had large intra-strut angles ranging from 40.21 to 50.00 degrees. Of the seven update points, six were non-dominated solutions and the remaining stent (S37) was unable to be constructed due to the lack of room for connectors.

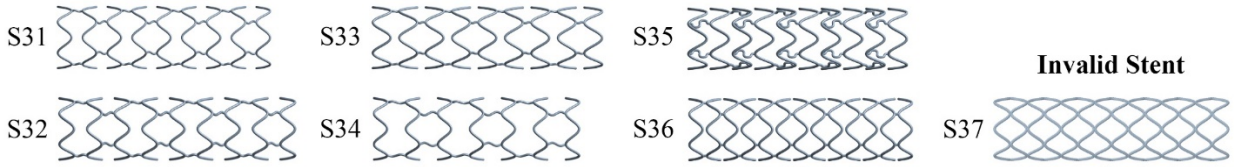

Figure 27. Six Constructed Updated Stents (Top) & One Invalid Stent (Bottom).

Table 6 outlines the measured haemodynamic and mechanical performance of each of the updated stent designs, where * marks an ND solution, ^ marks an objective or constraint that was used in the multi-objective process, and C refers to a circular cross-section. The remaining variables are explained in Table 1 of Section 3.2.1. Variable 'SD2' was removed from the table as only circular strutted designs were generated in the update process. The results for stress were based on the maximum loads applied which were 0.02MPa, 0.01N and 0.0004N for the radial, bending and compression simulations respectively. In addition, 'Inf" has been used to represent the result for the 1 invalid stent design.

Table 6. Performance of Updated Stent Designs.

#	CS	SD1 (μm)	SA (°)	AT (°)	CH (mm)	CT	NC	LWSS (% Area)	HWSS (% Area)^	TAWSS (% Area)^	Radial Stiffness (N/mm)^	Bending Stiffness (Nmm^2)	Comp Stiffness (N/mm)	Radial Stress (MPa)^	Bending Stress (MPa)	Comp Stress (MPa)
31*	C	99.52	49.073	180	1.2262	2	2	4.4696	72.5104	10.4110	3744.32	7.71114	0.36428	68.569	83.695	13.046
32*	C	119.97	47.271	180	1.3703	2	2	5.4549	66.6765	12.4982	5367.74	17.59730	0.74204	78.342	60.213	7.658
33*	C	113.05	41.387	180	1.3157	2	2	4.9562	69.8381	11.9031	3433.82	13.07536	0.56967	106.330	72.998	9.039
34*	C	110.96	50.000	180	1.5794	2	2	3.9418	75.5878	9.1626	3558.09	11.72404	0.71841	74.191	72.883	9.830
35*	C	119.79	40.210	0	1.1227	3	2	6.8267	58.7091	15.6360	3050.12	14.81365	0.57545	126.158	44.246	8.065
36*	C	120.00	49.999	180	0.8671	2	2	8.7037	59.3942	17.7310	10006.97	15.87796	0.58340	66.579	53.370	8.168
37	C	120.00	45.878	180	0.83	2	2	Inf	Inf	Inf	Inf	Inf	Inf	Inf	Inf	Inf

During the update process, a non-dominated solution from the initial sample, S11, became a dominated solution which means it did not have any objective values better than another design. This indicates that the optimisation approach was successfully producing stent designs that were non-dominated and improved upon the initial sample. 22 non-dominated solutions were identified from the entire sample, including the updated designs, and their objective values with respect to each other are illustrated in Figure 28. A trade-off between high WSS and low TAWSS was still identified and the updated stent results produced higher values of radial stiffness.

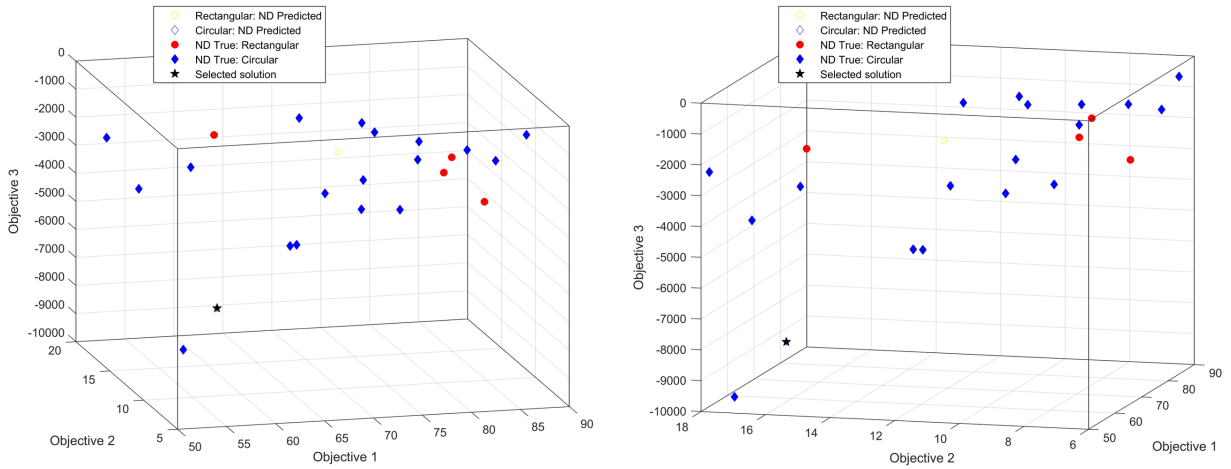

Figure 28. Comparison of Objective 1 (Minimising High WSS), Objective 2 (Minimising Low TAWSS), and Objective 3 (Maximising Radial Stiffness) for All 22 Non-Dominated Solutions.

4.3. Performance of the Non-Dominated Solutions

From the CFD simulations, the percentage of the area of low WSS, high WSS and low TAWSS was recorded and the results are illustrated in Figure 29 for the 22 non-dominated solutions. In this figure, WSS was restricted to be below 5 Pa and TAWSS was restricted to be below 4 Pa. The low TAWSS was shown to be predominately around the strut edges (shown in blue) and the point of connection between the stent cells and connectors, and the highest values of high WSS is shown predominantly along the strut faces, with lower high WSS values shown along the vessel wall in-between the struts at peak flow.

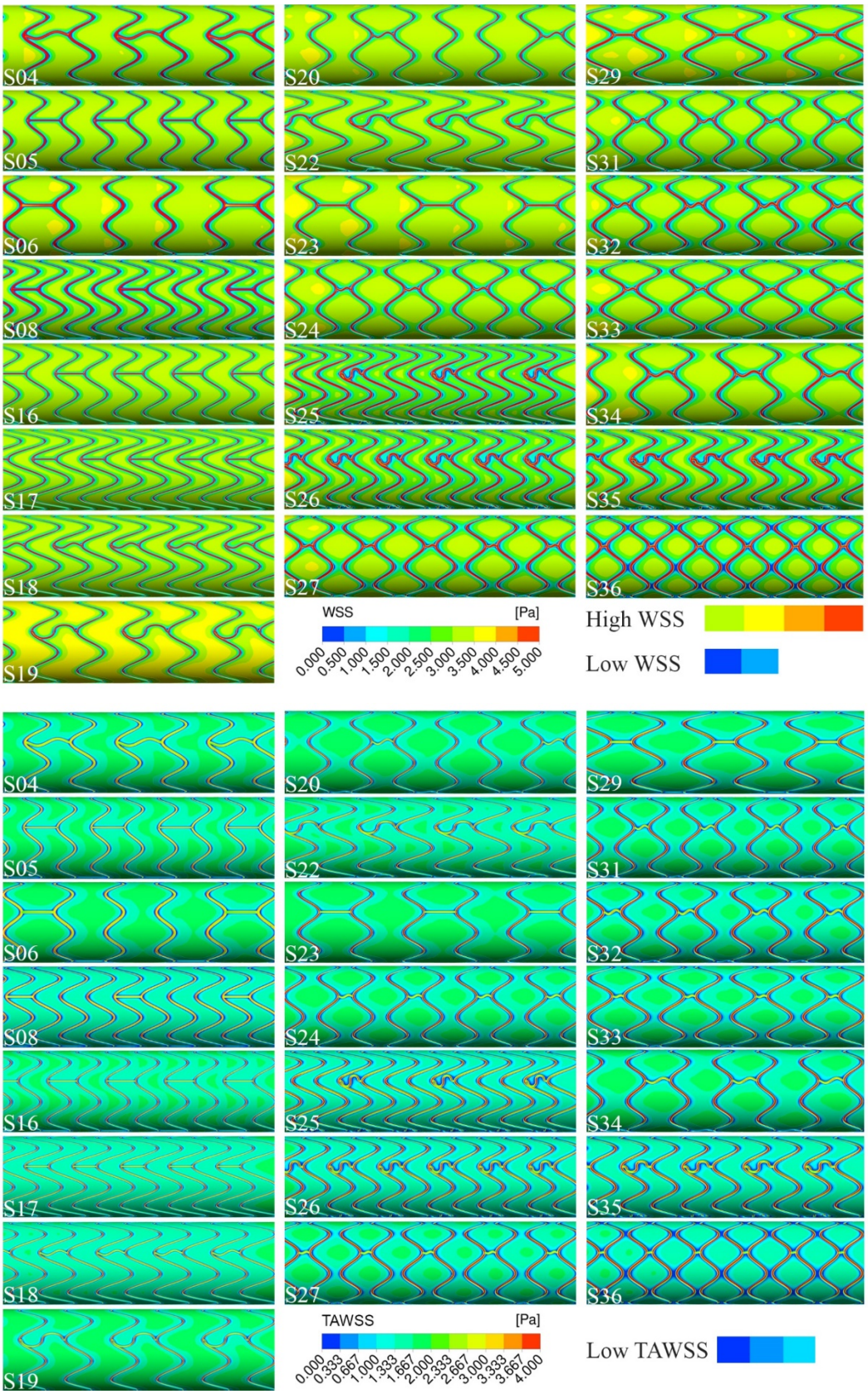

Figure 29. The WSS (Top) & TAWSS (Bottom) in CFX for 22 Non-Dominated Solutions.

From the FEA simulations, the deformation of the stent was recorded to calculate the radial stiffness, bending stiffness and compressive stiffness, and the deformation experienced by six of the 22 non-dominated solutions is illustrated in Figure 30. Across all of the stents, the maximum deformation is experienced by the centre cells and connectors in the bending simulation (the compressive deformation is shown in blue), and the maximum deformation is experienced by the cell and connectors at which the load was applied in the compressive simulation (shown in red). For the radial simulation, the total deformation was used in the results and the maximum deformation (shown in red) occurred at the peaks and for some connectors at a curved part, and the minimum deformation (shown in blue) typically was located at the valleys or at the cell's centre.

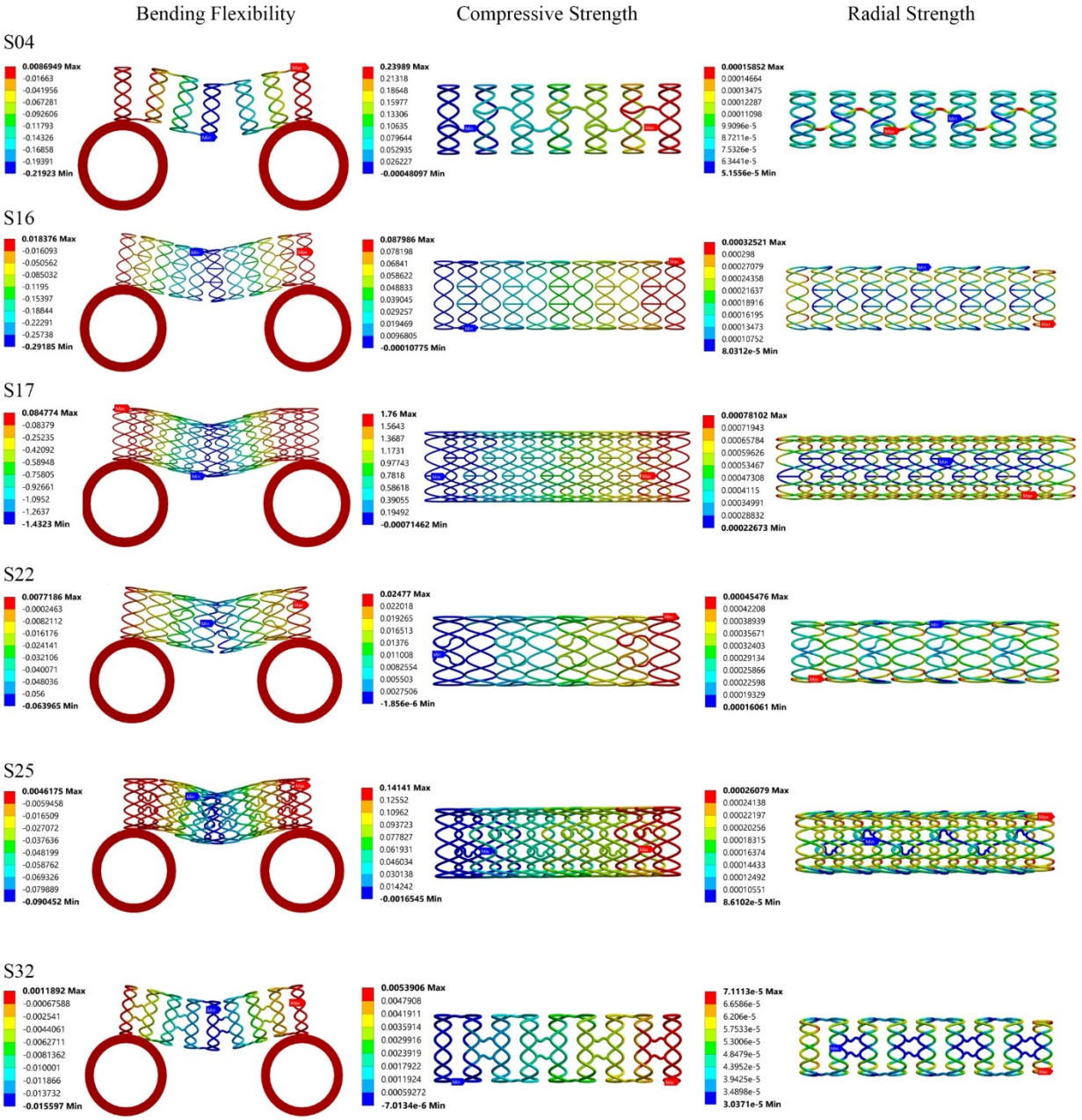

Figure 30. Deformation in FEA for 6 Non-Dominated Solutions (Auto-scaled).

Chapter 5 – Discussion

The aim of this study was to optimise stent design by analysing the effect of stent design variables on a stent's mechanical strength and effect on the local haemodynamic environment. Using the multi-objective optimisation process identified in Section 3.3, a sample of 30 initial stents were used to generate surrogates that would be iteratively updated and used to generate an additional seven stent designs. 17 non-dominated solutions were identified, and this increased to 22 non-dominated solutions after the update process. From the entire sample of stent designs, a total of five best performing designs were identified. Stent designs S19, S25 and S36 performed best in minimising low TAWSS, high WSS, and maximising the radial stiffness respectively. The ideal design point was defined as the lowest sum of square differences from the minimum measured objective values. Stent designs S11 and S32 were the closest designs to the ideal design point with rectangular and circular cross-sections respectively. Of these five best performing designs, only one design had a rectangular cross-section which suggests that stents with a circular cross-section performed better given the objectives for optimisation.

For these five best performing stents, the strut thickness ranged considerably from 73 μm to 120 μm, the cell height ranged considerably from 0.8495mm to 1.6685mm, and the strut angle ranged from 33.75° to 49.99° while the entire range of connector types, number of connectors and alignment types were exhibited. The sparse range in design variables for the five best performing designs indicates that there is a complex relationship between the design variables and objectives. For a comparison to the three other measured results, the three stent designs that minimised bending stiffness, low WSS, and maximised compressive stiffness (while experiencing stress below 2/3 of the yield stress) were identified to be S10, S19 and S29 respectively. Interestingly, the ideal stent design for low TAWSS was the same design for low WSS, confirming that these objectives are positively correlated. S10 and S29 had a cell height higher than the range established for the five best performing designs, and had one connector per cell and two connectors per cell respectively. These connector arrangements were expected as a lower number of connectors has been shown to increase bending flexibility while a greater number of connectors increases compressive strength [17] [20]. Hence, there is room in the future to expand this study and analyse the effect of the cell height and the number of connectors on the bending and compressive stiffness of stents.

The strut cross-section was identified to have a significant impact on the measured values of high WSS and low TAWSS. Illustrated in Figure 31, stents with a circular cross-section performed more favourably when compared to rectangular strutted stents which demonstrated a steep trade-off between TAWSS and WSS. This meant circular strutted stents produced a lower percentage of area with high WSS than rectangular strutted stents for the same percentage of area with low TAWSS. Therefore, it is evident that low TAWSS and high WSS are negatively correlated with a linear relationship, and this same relationship was identified between low WSS and high WSS. The circular strutted stents' favourable performance for two of the haemodynamic objectives explains why the optimisation algorithm identified only four rectangular strutted stents as non-dominated solutions out of the 22 and favoured circular strutted stents for the updated designs. As shown in Figure 31, there was no clear observed relationship between rectangular and circular strutted stents when comparing the radial stiffness to the low TAWSS and high WSS. However, it did show that low TAWSS generally increased as radial stiffness increased, while high WSS decreased

as radial stiffness increased but this relationship is not significant and was non-linear. While Putra et al. [26] compared triangular and rectangular strutted stents, rectangular and circular strutted stents have not been compared in previous studies. Given that there is only one current commercial stent with a circular cross-section, the results from this study suggests commercial stent design could be improved by changing to a circular cross-section.

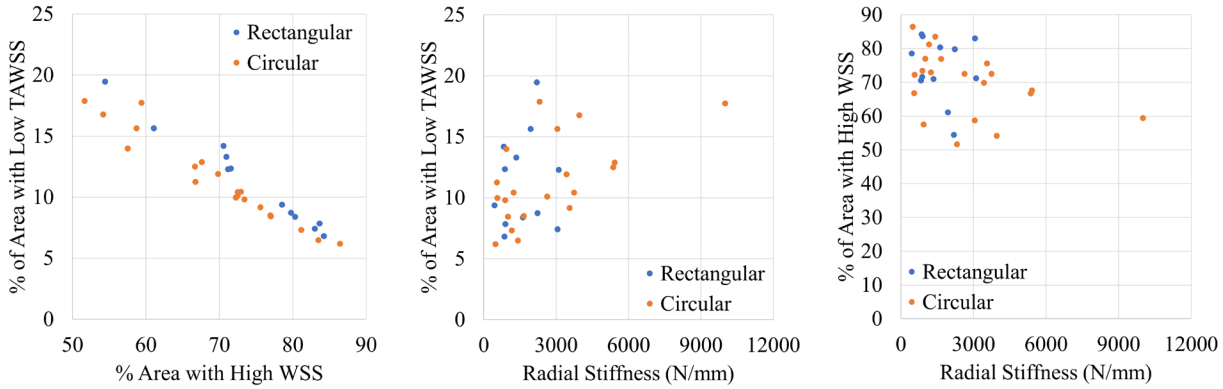

Figure 31. Comparison of Low TAWSS, High WSS, and Radial Stiffness for Circular and Rectangular Strutted Stents.

While it is often assumed that strut thickness is a direct indication of ideal hemodynamic performance, a comparison between the haemodynamic objectives and the strut dimension-to-cell height ratio identified a trade-off between strut thickness and cell height which agrees with Beier et al. [11]. A linear relationship was identified between the ratio and haemodynamic objectives as seen in Figure 32, which indicated that as the strut dimension-to-cell height ratio increases, the low TAWSS and low WSS increased, while high WSS decreased. The observed increase in adverse high WSS for smaller strut dimension-to-cell height ratios (thinner struts or larger cell heights) challenges the viewpoint of multiple studies that solely reducing strut thickness is haemodynamically beneficial [36]. Generally thinner struts that were less than 0.1mm performed the best in this study when considering low TAWSS, which is directly linked to intimal thickening and restenosis.

When considering the ratio of strut thickness (SD1)-to-cell height, Figure 32 illustrates that rectangular stents perform more favourably in regards to high WSS while circular stents perform more favourably in regards to low TAWSS. This suggests that rectangular stents may be preferred for more niche applications that prioritise minimizing high WSS, and hence reduce the risk of thrombosis. Importantly, if larger struts are required, the adverse haemodynamic effect of high WSS can be reduced with a smaller cell height. This relationship means a stent's structural integrity can be optimised without compromising its hemodynamic performance, but this may depend on vessel size [35]. It was found that the radial stiffness generally increased for circular strutted stents as the ratio of strut thickness (SD1)-to-cell height increased. For rectangular strutted stents, the radial stiffness was found to generally increase as the ratio of strut width (SD2)-to-cell height increased. As illustrated, the relationship between these variables is non-linear which is likely due to the high number of competing variables. Completing the same analysis for bending and compressive stiffness did not produce a notable relationship. Hence, this indicates that strut width predominantly contributes to the stent's radial strength as opposed to other mechanical objectives which agrees with the findings from Hsaio et al. [2].

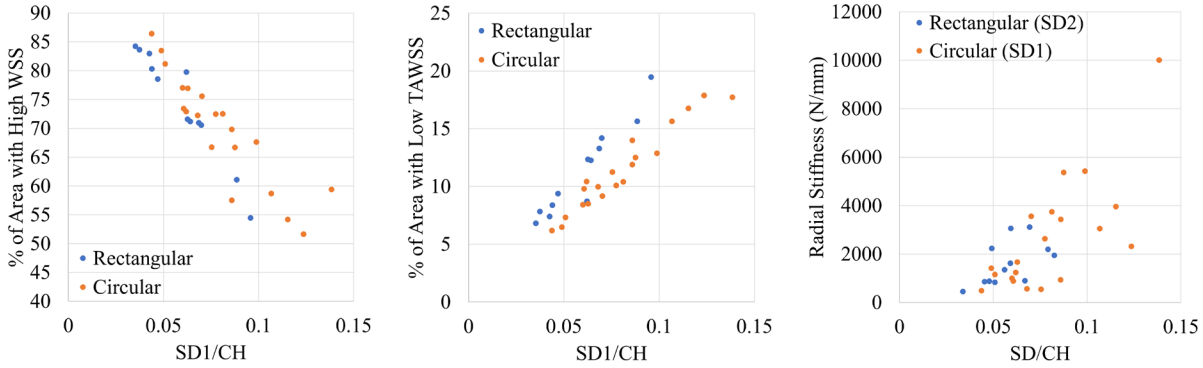

Figure 32. Comparison of High WSS (Left), Low TAWSS (Middle), and Radial Stiffness (Right) to the Strut Dimension – to – Cell Height Ratio for Circular and Rectangular Strutted Stents.

The number of connectors for each stent design had an important effect on all three objectives. As illustrated in Figure 33, it was found that having one connector per cell (labelled 1/1/1) performed the best for minimising low TAWSS, but performed the worst for minimising high WSS. The opposite performance was generally identified for stents with two connectors per cell (labelled 2/2/2) and stents with the 1/2/1 connectors arrangement. The decrease in the number of connectors was expected to have a haemodynamically beneficial effect based on the study by He et al. [22], however, stents with a lower number of connectors tended to benefit only one of the two haemodynamic objectives. While a lower number of connectors reduces the percentage of low TAWSS, Figure 34 identifies that stents with one connector per cell produce the lowest radial stiffness values. Only performing well in one objective (minimizing low TAWSS) is likely why the update process did not produce a single stent with one connector per cell. The measured mechanical characteristics were compared for each number of connectors as illustrated in Figure 34. Stents with two connectors per cell produced higher radial, bending and compressive stiffness compared to stents with one connector per cell. As expected, the stents with one connector per cell produced the lowest of these mechanical values, followed by stents with the 1/2/1 connector arrangement. Importantly, 10 out of the 22 identified non-dominated solutions produced bending stiffness values that were at least 500% greater (> 3 N/mm) than the smallest value measured and all of these stents had two connectors per cell. Future stent optimisation studies must consider minimising the bending stiffness as an objective to ensure flexibility of the stent [17] and include maximising compressive stiffness to ensure the stent's longitudinal strength is not sacrificed completely for this flexibility [23].

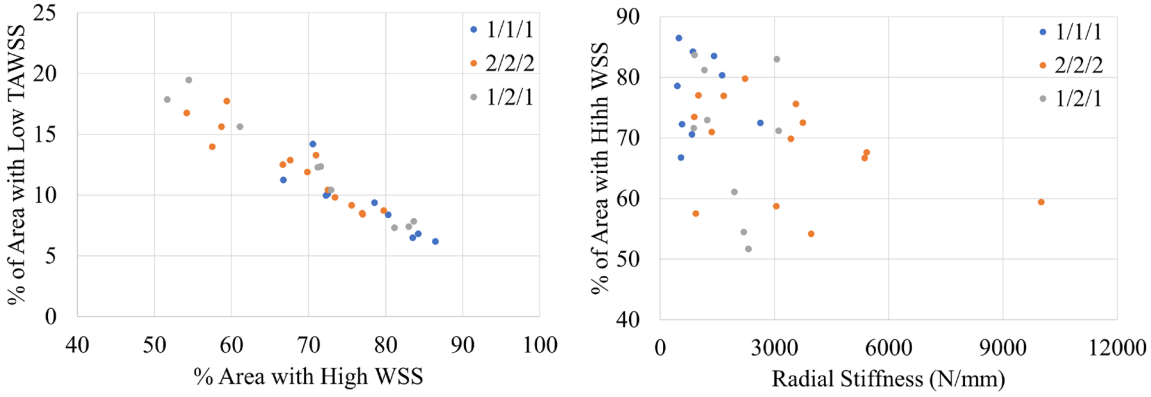

Figure 33. High WSS & Low WSS (Left), & high WSS & Radial Stiffness (Right) for the Number of Connectors.

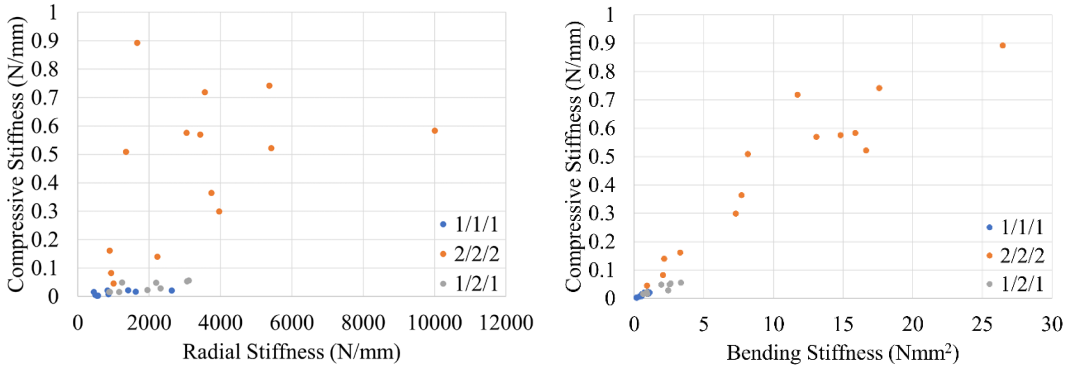

Figure 34. Compressive & Radial Stiffness (Left), & Bending Stiffness (Right) for the Number of Connectors.

Of all the 32 constructed stents, nine had straight connectors, 14 had spline connectors and nine had S-shape connectors. While studies have determined that the connectors should be aligned longitudinal to the flow to minimise flow misalignment [8] [22], the effect of different connector types on the high WSS and low TAWSS was not noticeably different. The majority of sampled stents with the highest radial, bending and compressive stiffness had spline connectors, closely followed by stents with S-shape connectors. Given the high radial stiffness associated with spline connectors, this explains why this connector type was predominantly selected by the optimisation algorithm for the update points. While six of the seven update points included an alignment of 180 degrees, this was not considered significant as half of all the 22 non-dominated solutions had an alignment of 0 degrees and half had 180 degrees, and hence the other design variables had more of an impact on the measured objectives. From the non-dominated solutions, the ideal range for the intra-strut angle was determined to be 29.58° to 50.00°. While this range may change for different vessel diameters [35], it reflects what is commercially available, so finding ideal stent designs within this range was expected. As the intra-strut angle increased, the radial stiffness generally increased, and this may explain why the update process preferred angles between 40.00° to 50.00° which agrees with the findings from Gundert et al. [34]. The inherent error of prediction was considered in the update process, and the updated designs performed favourably in terms of the radial stiffness and high WSS, but at the cost of low TAWSS.

The aim of this study was to provide general insights into stent design and the effect of certain variables on a stent's mechanical and haemodynamic performance. The study investigated the theoretical response of idealised stents and idealised stented vessel geometries, without in vivo characteristics such as lesions, patient-specific morphology, and stent deformation during deployment. Moreover, there may be an overestimation of the haemodynamic measured objectives as the blood vessel deformation was ignored [65]. Hence, rather than a clinical risk indication, this study provides a comparative insight on stent design. Outside of this study, there are other clinically relevant stent design variables including the stent diameter, the number of peaks, stent material, and the polymer and drug coating thickness, type and location. To improve the performance of stents, this study can be expanded in future works to consider more stent design variables and provide an optimisation on additional objectives including bending flexibility, compressive strength and minimising low WSS. The main contributions from this study include the identification of 22 ideal and novel stent designs and providing the haemodynamic and mechanical performance of a large range of stent geometric variations, those of which reflect commercial stents and idealised design variables from previous studies.

Chapter 6 – Part 2: Future Work

As explained in Section 3.1, this study is made of two Parts; Part 1 and Part 2. After completing Part 1 (Chapters 3, 4 and 5), substantial progress was made towards Part 2. Part 2 contains the future work which involves a larger stent optimisation process with a greater number of variables and objectives. The foundation for this future work was completed in this study in Part 2, which involved choosing the new variables and objectives, and constructing a completely new set of CAD modelled stents.

6.1. Stent Geometry

As explained in Section 3.2, a CAD model of each stent was constructed from the parameterised IronPython script that was developed in SpaceClaim API V18 ANSYS 19.2. Each stent was generated from the design constraints outlined in Section 3.2.2, excluding the material and number of peaks constraint, and the following design variables.

6.1.1. Design Variables

Two more significant stent design variables and new design constraint ranges were identified from the literature review, and these are to be investigated in future work on stent design optimisation with a total of 10 design variables. These 10 design variables include the eight design variables discussed in Section 3.2.1, and additionally the stent's material, and the number of peaks. Moreover, a new design constraint range was assigned for the number of connectors and connector types. There were 10 design variables and nine design variables for the rectangular and circular cross-sections respectively. The 10 design variables and constraint ranges for the future work are given in Table 7.

Table 7. The Stent Design Variables and Constraint Range for Future Work.

Variables	Design Range
Cross-Sectional Shape (CS)	Rectangular or Circular
Strut Dimension 1 (SD1, Strut Thickness or Diameter)	60 μm - 120 μm
Strut Dimension 2 (SD2, Strut Width)	60 μm - 120 μm
Intra-Strut Angle (SA)	25° - 50°
Alignment Type (AT)	0° or 180°
Cell Height (CH)	0.83 mm – 2.00 mm
Connector Type (CT)	Straight, Spline, Semi-Circular (S-Shape), M-Shape, alternating Straight/Spline, or alternating Straight/M-Shape
Number of Connectors (NC)	2 per cell, 3 per cell, or 3/3/3/ (proximal cells) followed by 2 per cell
Number of peaks (NP)	6, 7, 8, or 9
Material	Platinum Chromium or L-605 Cobalt-Chromium

Based on what was commercially available, the number of peaks was added as a design variable due to its significant impact on flow misalignment, and hence the haemodynamic environment [11] [35]. The number of peaks and stent diameter are inter-connected, and the stent geometry script was designed to expand this future work to explore the effect of changing the stent diameter, specifically looking at 2.5mm, 3mm and 4mm based on studies such as Plitt et

al. [29]. In the interest of the mechanical design objectives, the material of the stent was added as a design variable to compare two materials used in current commercial stents [20]. Illustrated in Figure 35, three new connector types (M-shape, alternating Straight/Spline, alternating Straight/M-shape) were also added to the existing types to investigate other commercial stent designs and examine the effect of alternating between flex and non-flex connectors between cells. The parametrised equation developed to define the M-shape connector is shown in Table 8.

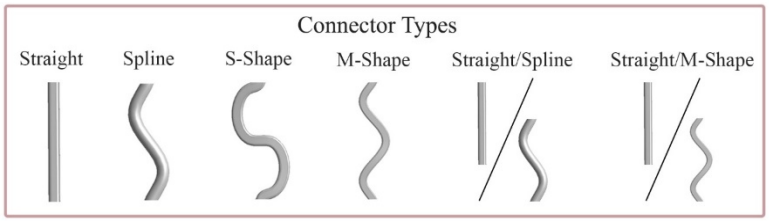

Figure 35. Connector Types for Future Work.

Table 8. M-Shape Connector Type Equation for Future Work.

Connector Type	Equation
M-Shape	$f(z) = \{0 \leq z \leq 1 \ : \ c_1 \cdot z^2(1-z)^2(0.333-z)(0.666-z)\}$ $Where\ 0 < c_1 \leq 100$

The design constraint range for the number of connectors was changed to include designs that were more reflective of commercial stents, ensuring a minimum of two connectors per cell to improve longitudinal strength [17]. Moreover, the effect of having a greater number of connectors at the proximal cells of the stent would be investigated. To ensure the connector arrangement pattern created a stent which is as stable as possible, the pattern for each number of connectors was designed to be dependent on the number of peaks and is illustrated in Figure 36.

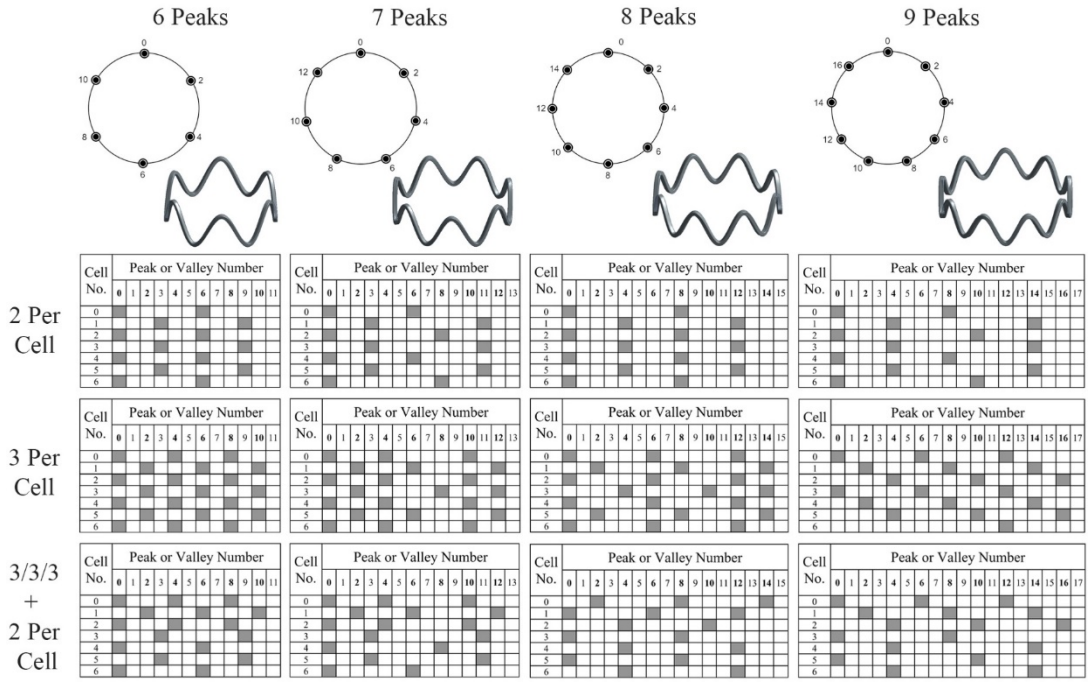

Figure 36. Connector Arrangement for 6, 7, 8 & 9 Peaks in Future Work (Peaks are in Bold).

6.2. Multi-Objective Optimisation Process

As discussed in Section 6.1.1, the stent design variables were further developed and included in the IronPython script for future work. Progress was made towards the optimisation of stents based on these developed design variables. The exact optimisation method discussed in Section 3.3 will be adopted in future work however six objectives and three constraints will be considered rather than three and one respectively. Moreover, the optimisation algorithm NSGA-II may not be suitable for more than three objectives and may need to be adjusted. The objectives (three from CFD and three from FEA) were defined as follows;

1. $Minimise\ the\ \%\ of\ Area\ with\ Low\ WSS$
2. $Minimise\ the\ \%\ of\ Area\ with\ High\ WSS$
3. $Minimise\ the\ \%\ of\ Area\ with\ Low\ TAWSS$
4. $Minimise\ the\ Bending\ Stiffness$
5. $Maximise\ the\ Radial\ Stiffness$
6. $Maximise\ the\ Compressional\ Stiffness$

The mechanical constraints to be considered are defined as follows;

$$Bending\ Maximum\ Stress \leq \frac{2}{3} \times Yield\ Stress$$

$$Radial\ Maximum\ Stress \leq \frac{2}{3} \times Yield\ Stress$$

$$Compressional\ Maximum\ Stress \leq \frac{2}{3} \times Yield\ Stress$$

For the materials to be considered in the future work, the maximum stress any stent could experience is 333.333 MPa [70] for stents made of L-605 cobalt-chromium, and 320 MPa [73] for stents made of Platinum Chromium.

6.2.1. Sample of Stent Designs

Based on the number of design variables (10) and objectives (6), a sample of 60 design points was considered suitable. A sample containing 60 stent designs was generated using the Latin Hypercube Sampling approach and the specific design constraint range for each is recorded in Table 9 in Appendix B. As illustrated in Figure 37, the sample of 60 stents was constructed, and of the 60 stents, four of the stents were unable to be generated due to the physical, geometric impossibilities of the design. Hence, these models were disregarded, and the 56 successfully created stents were saved and set aside to be used in future work.

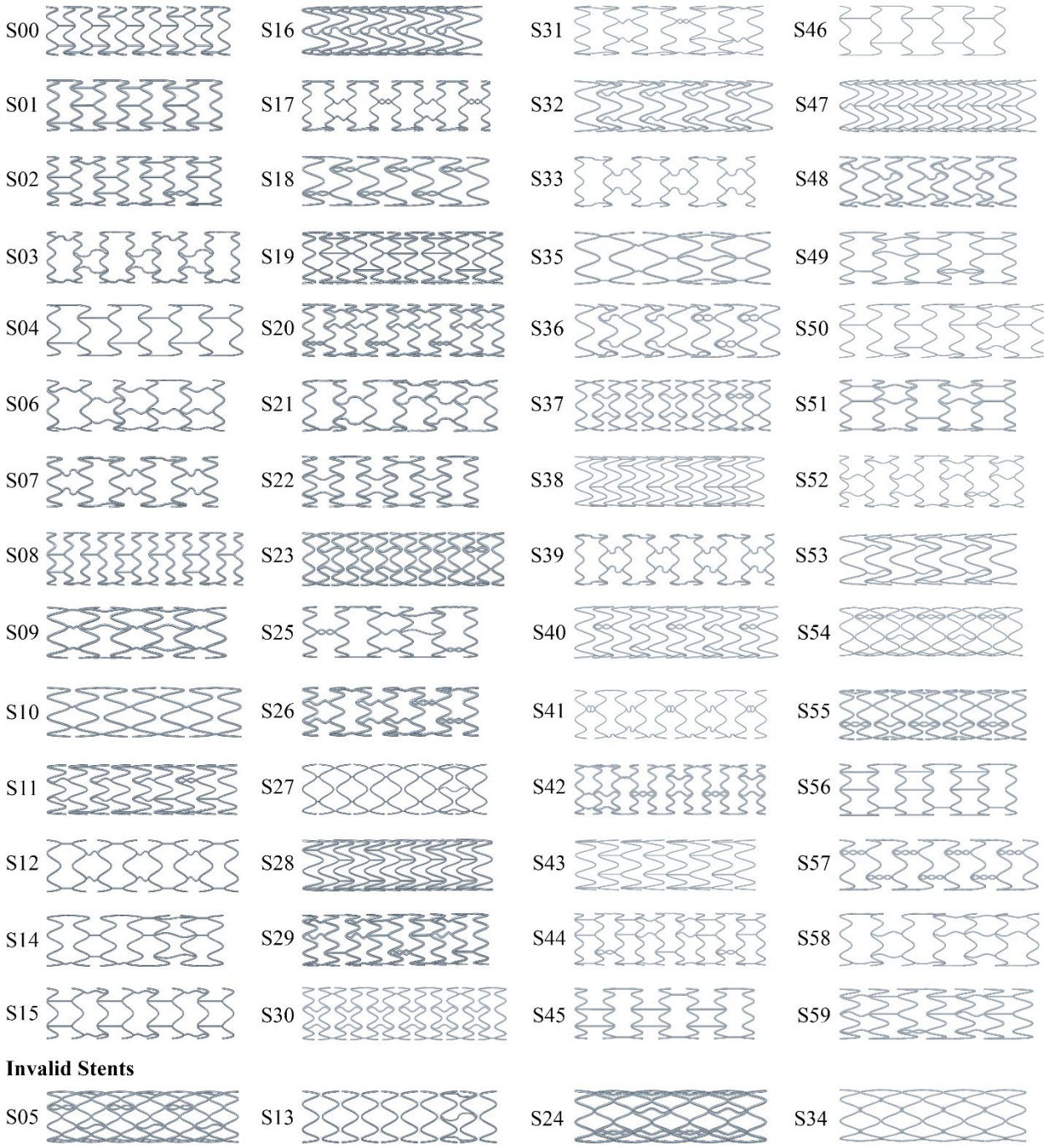

Figure 37. 56 Constructed Stents (Top) & Four Invalid Stents (Bottom) for Future Work.

Chapter 7 - Conclusion

The aim of this study was to improve stent design by analysing the complex relationship between stent design variables and a stent's mechanical and haemodynamic performance. A multi-objective optimisation of stent design was completed using eight major stent design variables and three key stent performance objectives that build and improve on a substantial preceding literature. A stent's adverse effect on the haemodynamic environment has been linked to low WSS, low TAWSS and high WSS, while a stent's mechanical failure is dependent on its radial, compressive and bending stiffness. Multiple studies have endeavoured to optimise stent design with either haemodynamic or mechanical considerations and consider only a limited number of variables. Of the minimal studies that investigate both mechanical and haemodynamic performance outcomes, only four or fewer design variables were investigated individually. Hence, this work strived to expand on this literature and provide an optimisation of stents for multiple design variables and for both haemodynamic and mechanical objectives.

Using a Latin Hypercube Sampling approach, an initial set of 30 novel stent designs were computationally modelled to acquire their haemodynamic and mechanical performance using CFD and FEA respectively. The results from these simulations were used to inform an optimisation algorithm, NSGA-II with EHVI, which then predicted six new non-dominated, ideal stent designs. From the entire sample of generated stents, the five best performing stents and 22 non-dominated solutions were identified. These are 22 completely new stent designs which are likely superior to any commercially available stents to date given that these new designs were developed from design variables that were based on commercial stents. The main findings from this study included the favourable haemodynamic performance of circular-strutted stents, the trade-off between cell height and strut thickness, and the beneficial mechanical effect of more connectors on the radial and compressive stiffness. Given the great increase in radial stiffness for stents with two connectors per cell and the improvement in both haemodynamic objectives for circular strutted stents, the update process was deemed successful in improving stent design based on the six ideal stent designs it generated.

Substantial progress was made towards future work by expanding this study to consider 10 significant stent design variables and six objectives. Given the compressive strength and flexibility required of stents during deployment, this study confirmed that consideration of a stent's bending and compressive stiffness needs to be accounted for in the multi-objective optimisation process to ensure a balance between too many and too few connectors. Based on literature and commercial designs, the new design variables were expanded to include the stent material, number of peaks, and new connector types and arrangements. Based on these new variables and objectives, a Latin Hypercube sample of 60 stents were generated and computationally modelled. This study could be further expanded to investigate the effect of different stent diameters as this is closely related to the number of peaks. Using this study as its foundation, future work will ideally be able to provide ideal, balanced stent designs that consider the low WSS, bending stiffness and compressive stiffness in addition to the current haemodynamic and mechanical performance objectives. Overall, this study was successful in identifying 22 novel stent designs based on the haemodynamic and mechanical performance of a large range of generated stent geometries, and will likely result in new, better-performing stent designs for commercial use. Importantly, this study analysed the effect of significant design variables on competing objectives which will inform and influence future work and assist in developing balanced and improved stent designs.

References

[1] D. Hoare, A. Bussooa, S. Neale, N. Mirzai and J. Mercer, "The Future of Cardiovascular Stents: Bioresorbable and Integrated Biosensor Technology," *Advanced Science,* vol. 6, no. 20, p. 1900856, 2019.

[2] H.-M. Hsiao, C. Yi-Hsiang, L. Kuang-Huei and L. Chien-Han, "Computational modeling of effects of intravascular stent design on key mechanical and hemodynamic behaviour," *Computer-aided design,* vol. 44, no. 8, pp. 757-765, 2012.

[3] A. Qiao, F. Yulin and Z. Zhanzhu, "Research of Numerical Simulation of Biomechanics on In-stent-restenosis," *J. Vasc. Med. Surg.,* vol. 3, no. 1, pp. 1-5, 2015.

[4] F. Alfonso, R. A. Byrne, F. Rivero and A. Kastrati, "Current Treatment of In-Stent Restenosis," *Journal of the American College of Cardiology,* vol. 63, no. 24, pp. 2659-2673, 2014.

[5] A. Fortier, V. Gullapalli and A. R. Mirshams, "Review of biomechanical studies of arteries and their effect on stent performance," *IJC Heart & Vessels,* vol. 4, pp. 12-18, 2014.

[6] J. Iqbal, J. Gunn and P. W. Serruys, "Coronary stents: historical development, current status and future directions," *British medical bulletin,* vol. 106, no. 1, pp. 193-211, 2013.

[7] N. Pal, J. Din and P. O'Kane, "Contemporary Management of Stent Failure: Part One," *Cardiology Review,* vol. 14, no. 1, pp. 10-16, 2019.

[8] S. Pant, N. W. Bressloff, A. I. J. Forrester and N. Curzen, "The Influence of Strut-Connectors in Stented Vessels: A Comparison of Pulsatile Flow Through Five Coronary Stents," *Annals of biomedical engineering,* vol. 38, no. 5, pp. 1893-1907, 2010.

[9] S. Windecker and B. Meier, "Late Coronary Stent Thrombosis," *Circulation,* vol. 116, no. 17, pp. 1952-1965, 2007.

[10] M. Iannaccone, P. Gatti, U. Barbero, A. Bassignana, D. Gallo, M. De Benedictis, G. Helft, U. Morbiducci, B. Doronzo and F. D'Ascenzo, "Impact of Strut Thickness and Number of Crown and Connectors on Clinical Outcomes on Patients Treated with Second-Generation Drug Eluting Stent," *Catheterization and Cadriovascular Interventions,* pp. 1-6, 2019.

[11] S. Beier, J. Ormiston, M. Webster, J. Cater, S. Norris, P. Medrano-Gracia, A. Young and B. Cowan, "Hemodynamics in Idealized Stented Coronary Arteries: Important Stent Design Considerations," *Annals of biomedical engineering,* vol. 44, no. 2, pp. 315-329, 2016.

[12] J. F. LaDisa Jr, L. E. Olson, R. C. Molthen, D. A. Hettrick, P. F. Pratt, M. D. Hardel, J. R. Kersten, D. C. Warltier and S. P. Pagel, "Alterations in wall shear stress predict sites of neointimal hyperplasia after stent implantation in rabbit iliac arteries," *American Journal of Physiology-Heart and Circulatory Physiology ,* vol. 288, no. 5, pp. H2465-H2475, 2005.

[13] A. M. Malek, S. L. Alper and S. Izumo, "Hemodynamic Shear Stress and Its Role in Atherosclerosis," *Jama,* vol. 282, no. 21, pp. 2035-2042, 1999.

[14] G. Frank, Y. Katagiri, P. Barlis, C. Bourantas, C. Collet, U. Coskun, J. Daemen, J. Dijkstra, E. Edelman, P. Evans, K. Van der Heiden, R. Hose, B.-K. Koo, R. Krams, A. Marsden, F. Migliavacca, Y. Onuma, A. Ooi, E. Poon, H. Samady, P. Stone, K. Takahashi, D. Tang, V. Thondapu, E. Tenekecioglu, L. Timmins, R. Torii, J. Wentzel and P. Serruys, "Expert recommendations on the assessment of wall shear stress in human coronary arteries: existing methodologies, technical considerations, and clinical applications," *European Heart Journal,* vol. 40, no. 41, pp. 3421-3433, 2019.

[15] H. Samady, P. Eshtehardi, M. C. McDaniel, J. Suo, S. S. Dhawan, C. Maynard, L. H. Timmins, A. A. Quyyumi and D. P. Giddens, "Coronary Artery Wall Shear Stress is Associated with Progression and Transformation of Atherosclerotic Plaque and Arterial Remodeling in Patients with Coronary Arterty Disease," *Circulation,* vol. 124, no. 7, pp. 779-788, 2011.

[16] J. M. Dolan, J. Kolega and H. Meng, "High wall shear stress and spatial gradients in vascular pathology: a review," *Annals of biomedical engineering,* vol. 41, no. 7, pp. 1411-1427, 2013.

[17] J. A. Ormiston, B. Webber, B. Ubod, J. White and M. W. Webster, "Coronary stent durability and fracture: an independent bench comparison of six contemporary designs using a repetitive bend test," *EuroIntervention: journal of EuroPCR in collaboration with the Working Group on Interventional Cardiology of the European Society of Cardiology,* vol. 10, no. 12, pp. 1449-1455, 2015.

[18] M. Ferraro, "Advanced Modeling of Stents: from constitutive modeling to biomedical (isogeometric) analysis," Doctoral dissertation, PhD thesis, 2014.

[19] S. Muller-Hulsbeck, P. J. Schafer, N. Charalambous, H. Yagi, M. Heller and T. Jahnke, "Comparison of Second-Generation Stents for Application in the Superficial Femoral Artery: In Vitro Evaluation Focussing on Stent Design," *Journal of Endovascular Therapy,* vol. 17, no. 6, pp. 767-776, 2010.

[20] T. Watson, M. W. Webster, J. A. Ormiston, P. N. Ruygrok and J. T. Stewart, "Long and short of optimal stent design," *Open heart,* vol. 4, no. 2, pp. 1-6, 2017.

[21] S. Torii, H. Jinnouchi, A. Sakamoto, M. Kutyna, A. Cornelissen, S. Kuntz, L. Guo, H. Mori, E. Harari, K. H. Paek and R. Fernandez, "Drug-eluting coronary stents: insights from preclinical and pathology studies," *Nature Reviews Cardiology,* vol. 17, no. 1, pp. 37-51, 2020.

[22] Y. He, N. Duraiswamy, A. O. Frank and J. E. Moore Jr, "Blood flow in stented arteries: a parametric comparison of strut design patterns in three dimensions," *Journal of Biomechanical Engineering,* vol. 127, pp. 637-647, 2005.

[23] Z. M. Xie, X. Shen, Y. Q. Deng and S. Ji, "Effects of metal material stent design parameters on longitudinal stent strength," *In Key Engineering Materials,* vol. 723, no. Trans Tech Publications, pp. 299-304, 2017.

[24] H. Huang, J. Yan, V. Bhat and M. Sirhan, "Intravascular Stent". U.S. Patent 12/965,080, 18 February 2016.

[25] J. M. Jimenez and P. F. Davies, "Hemodynamically driven stent strut design," *Annals of biomedical engineering,* vol. 37, no. 8, pp. 1483-1494, 2009.

[26] N. K. Putra, P. S. Palar, H. Anzai, K. Shimoyama and M. Ohta, "Multiobjective design optimization of stent geometry with wall deformation for triangular and rectangular struts," *Medical & biological engineering & computing,* vol. 57, no. 1, pp. 15-26, 2019.

[27] E. K. Poon, P. Barlis, S. Moore, W.-H. Pan, Y. Liu, Y. Ye, Y. Xue, S. J. Zhu and A. S. Ooi, "Numerical investigations of the haemodynamic changes associated with stent malapposition in an idealised coronary artery," *Journal of biomechanics,* vol. 47, no. 12, pp. 2843-2851, 2014.

[28] K. Nisbett and R. G. Budynas, Shigley's Mechanical Engineering Design, 10th Edition, 2015.

[29] A. Plitt, B. E. Claessen, S. Sartori, U. Baber, J. Chandrasekhar, M. Aquino, P. Vijay, S. Elsayed, J. C. Kovacic, J. Sweeny, N. Barman, P. Moreno, P. Krishnan, A. Demopoulos, G. Dangas, A. S. Kini, R. Mehran and S. K. Sharma, "Impact of stent diameter on outcomes following percutaneous coronary intervention with second-generation drug-eluting stents: Results from a large single-center registry," *Catheterization and Cardiovascular Interventions,* pp. 1-7, 2019.

[30] J. Wiebe, P. Hoppmann, S. Kufner, Y. Harada, R. Colleran, J. Michel, D. Giacoppo, S. Schneider, S. Cassese, T. Ibrahim, H. Schunkert, K.-L. Laugwitz, A. Kastrati and R. A. Byrne, "Impact of stent size on angiographic and clinical outcomes after implantation of everolimus-eluting bioresorbable scaffolds in daily practice: insights from the ISAR-ABSORB registry," *EuroIntervention: journal of EuroPCR in collaboration with the Working Group on Interventional Cardiology of the European Society of Cardiology,* vol. 12, no. 2, pp. e137-43, 2016.

[31] H. Kitahara, K. Okada, T. Kimura, P. G. Yock, A. J. Lanskey, J. J. Popma, A. C. Yeung, P. J. Fitzgerald and Y. Honda, "Impact of stent size selection on acute and long-term outcomes after drug-eluting stent implantation in de novo coronary lesions," *Circulation: Cardiovascular Interventions,* vol. 10, no. 10, p. e004795, 2017.

[32] D. H. Steinberg, S. Mishra, A. Javaid, T. L. P. Slottow, A. N. Buch, P. Roy, T. Okabe, K. A. Smith, R. Torguson, Z. Xue, A. D. Pichard, L. F. Satler, K. M. Kent, W. O. Suddath and R. Waksman, "Comparison of effectiveness of bare metal stents versus drug-eluting stents in large (≥ 3.5 mm) coronary arteries," *The American journal of cardiology,* vol. 99, no. 5, pp. 599-602, 2007.

[33] R. Zbinden, S. von Felten, B. Wein, D. Tueller, D. J. Kurz, I. Reho, S. Galatius, H. Alber, D. Conen, M. Pfisterer, C. Kaiser and F. R. Eberli, "Impact of stent diameter and length on in-stent restenosis after DES vs BMS implantation in patients needing large coronary stents—A clinical and health-economic evaluation," *Cardiovascular therapeutics,* vol. 35, no. 1, pp. 19-25, 2017.

[34] T. J. Gundert, A. L. Marsden, W. Yang and J. F. LaDisa, "Optimization of cardiovascular stent design using computational fluid dynamics," *Journal of biomechanical engineering,* vol. 134, no. 1, pp. 011002-1-011002-8, 2012.

[35] T. J. Gundert, A. L. Marsden, W. Yang, D. S. Marks and J. F. LaDisa Jr, "Identification of hemodynamically optimal coronary stent designs based on vessel caliber," *IEEE Transactions on Biomedical Engineering,* vol. 59, no. 7, pp. 1992-2002, 2012.

[36] A. Kastrati, J. Mehilli, J. Dirschinger, F. Dotzer, H. Schuhlen, F.-J. Neumann, M. Fleckenstein, C. Pfafferott, M. Seyfarth and A. Schomig, "Intracoronary stenting and angiographic results: strut thickness effect on restenosis outcome (ISAR-STEREO) trial," *Circulation,* vol. 103, no. 23, pp. 2816-2821, 2001.

[37] N. K. Putra, P. S. Palar, H. Anzai, K. Shimoyama and M. Ohta, "Stent design optimization based on Kriging surrogate model under deformed vessel wall: pulsatile inlet flow," *In 2017 5th International Conference on Instrumentation, Control, and Automation (ICA),* pp. 172-176, 2017.

[38] P. D. Williams, M. A. Mamas, K. P. Morgan, M. El-Omar, B. Clarke, A. Bainbridge, F. Fath-Ordoubadi and D. G. Fraser, "Longitudinal stent deformation: a retrospective analysis of frequency and mechanisms," *EuroIntervention: journal of EuroPCR in collaboration with the Working Group on Interventional Cardiology of the European Society of Cardiology,* vol. 8, no. 2, pp. 267-274, 2012.

[39] M. Pitney, K. Pitney, N. Jepson, D. Friedman, T. Nguyen-Dang, J. Matthews, R. Giles and D. Taylor, "Major stent deformation/pseudofracture of 7 Crown Endeavor/Micro Driver stent platform: incidence and causative factors," *EuroIntervention: journal of EuroPCR in collaboration with the Working Group on Interventional Cardiology of the European Society of Cardiology,* vol. 7, no. 2, pp. 256-262, 2011.

[40] K. Iwasaki, S. Kishigami, J. Arai, T. Ohba, X. Zhu, T. Yamamoto, Y. Hikichi and M. Umezu, "Flexibility and Stent fracture potentials against cyclically bending coronary artery motions: comparison between 2-link and 3-link DESs," *American Journal of Cardiology,* vol. 111, no. 7, p. 26B, 2013.

[41] N. W. Bressloff, G. Ragkousis and N. Curzen, "Design optimisation of coronary artery stent systems." Annals of biomedical engineering," *Annals of biomedical engineering,* vol. 44, no. 2, pp. 357-367, 2016.

[42] L. Hongxia, T. Qiu, B. Zhu, J. Wu and X. Wang, "Design optimization of coronary stent based on finite element models," *The Scientific World Journal ,* pp. 1-10, 2013.

[43] M. A. Atherton and R. A. Bates, "Robust optimization of cardiovascular stents: a comparison of methods," *Engineering Optimization,* vol. 36, no. 2, pp. 207-217, 2004.

[44] N. K. Putra, P. S. Palar, H. Anzai, K. Shimoyama and M. Ohta, "Comparative study between different strut's cross section shape on minimizing low wall shear stress along stent vicinity via Surrogate-based optimization," *World Congress of Structural and Multidisciplinary Optimisation,* pp. 2097-2109, 2017.

[45] L. H. Timmins, M. R. Moreno, C. A. Meyer, J. C. Criscione, A. Rachev and J. E. Moore, "Stented artery biomechanics and device design optimization," *Medical & Biological Engineering & Computing,* vol. 45, no. 5, pp. 505-513, 2008.

[46] R. Clune, D. Kelliher, J. C. Robinson and J. S. Campbell, "NURBS modeling and structural shape optimization of cardiovascular stents.," *Structural and Multidisciplinary Optimization,* vol. 50, no. 1, pp. 159-168, 2014.

[47] S. Pant, N. W. Bressloff and G. Limbert, "Geometry parameterization and multidisciplinary constrained optimization of coronary stents," *Biomechanics and modeling in mechanobiology,* vol. 11, no. 1-2, pp. 61-82, 2012.

[48] S. Tammareddi, G. Sun and Q. Li, "Multiobjective robust optimization of coronary stents," *Materials & Design,* vol. 90, pp. 682-692, 2016.

[49] S. Pant, G. Limbert, N. P. Curzen and N. W. Bressloff, "Multiobjective design optimisation of coronary stents," *Biomaterials,* vol. 32, no. 31, pp. 7755-7773, 2011.

[50] A. Qiao, Y. Fu and Z. Zhang, "Research of Numerical Simulation of Biomechanics on In-stent-restenosis," *J. Vasc. Med. Surg.,* vol. 3, no. 1, pp. 1-5, 2015.

[51] P. Nasim, D. S. Cronin and P. Lee-Sullivan, "Finite element methods to analyze helical stent expansion," *International Journal for numerical methods in biomedical Engineering,* vol. 30, no. 3, pp. 339-352, 2014.

[52] F. Migliavacca, L. Petrini, M. Colombo, F. Auricchio and R. Pietrabissa, "Mechanical behavior of coronary stents investigated through the finite element method," *Journal of biomechanics,* vol. 35, no. 6, pp. 803-811, 2002.

[53] Q. Wang, G. Fang, Y. Zhao, G. Wang and T. Cai, "Computational and experimental investigation into mechanical performances of Poly-L-Lactide Acid (PLLA) coronary stents," *Journal of the mechanical behavior of biomedical materials,* vol. 65, pp. 415-427, 2017.

[54] A. Schiavone, "Computational Modelling of Stent Deployment and Mechanical Performance Inside Human Atherosclerotic Arteries, A Doctoral Thesis," Alessandro Schiavone, 2015.

[55] J. A. Ormiston, B. Webber and M. W. Webster, "Stent longitudinal integrity: bench insights into a clinical problem," *ACC: Cardiovascular Interventions,* vol. 4, no. 12, pp. 1310-1317, 2011.

[56] T. R. Choundhury, S. Al-Saigh, S. Burley, L. Li, N. Shakhshir, N. Mirhosseini, T. Wang, S. Arnous, M. A. Khan, A. M. Mamas and D. G. W. Fraser, "Longitudinal deformation bench testing using a coronary artery model: a new standard?," *Open Heart,* vol. 4, no. 2, p. e000537, 2017.

[57] G. Leibundgut, M. Gick, A. Toma, C. Valina, N. Loffelhardt, H. J. Buttner and F.-J. Neumann, "Longitudinal compression of the platinum-chromium everolimus-eluting stent during coronary implantation: Predisposing mechanical properties, incidence, and predictors in a large patient cohort," *Catheterization and Cardiovascular Interventions,* vol. 81, no. 5, pp. E206-E214, 2013.

[58] Q. Wang, G. Fang, Y.-H. Zhao and J. Zhou, "Improvement of mechanical performance of bioresorbable magnesium alloy coronary artery stents through stent pattern redesign," *Applied Sciences,* vol. 8, no. 12, p. 2461, 2018.

[59] A. Kumar, R. Ahuja, P. Bhati, P. Vashisth and N. Bhatnagar, "Design Methodology of a Balloon Expandable Polymeric Stent," *Journal of Biomed Engineering and Medical Devices,* vol. 4, no. 1, pp. 1-17, 2019.

[60] A. Borghi, O. Murphy, R. Bahmanyar and C. McLeod, "Effect of stent radial force on stress pattern after deployment: a finite element study," *Journal of materials engineering and performance,* vol. 23, no. 7, pp. 2599-2605, 2014.

[61] X.-Y. Ni, C.-W. Pan and B. Gangadhara Prusty, "Numerical investigations of the mechanical properties of a braided non-vascular stent design using finite element method," *Computer methods in biomechanics and biomedical engineering,* vol. 18, no. 10, pp. 1117-1125, 2015.

[62] D. Yoshino, K. Inoue and Y. Narita, "Understanding the mechanical properties of self-expandable stents: a key to successful product development," *Journal of Mechanical Engineering,* vol. 6, no. 54, pp. 471-485, 2008.

[63] A. C. Bobel, S. Petisco, J. R. Sarasua, W. Wang and P. E. McHugh, "Computational bench testing to evaluate the short-term mechanical performance of a polymeric stent," *Cardiovascular engineering and technology,* vol. 6, no. 4, pp. 519-532, 2015.

[64] R. Balossino, F. Gervaso, F. Migliavacca and G. Dubini, "Effects of different stent designs on local hemodynamics in stented arteries," *Journal of biomechanics 41,,* vol. 41, no. 5, pp. 1053-1061, 2008.

[65] C. Chiastra, F. Migliavacca, M. A. Martinez and M. Malve, "On the necessity of modelling fluid–structure interaction for stented coronary arteries," *Journal of the mechanical behavior of biomedical materials,* vol. 34, pp. 217-230, 2014.

[66] J. Meija, R. Mongrain and O. F. Bertrand, "Accurate prediction of wall shear stress in a stented artery: Newtonian versus non-Newtonian models," *Journal of biomechanical engineering,* vol. 133, no. 7, pp. 074501-1-074501-8, 2011.

[67] W. Nichols, M. F. O'Rourke and C. Vlachopoulos, McDonald's Blood Flow in Arteries: Theoretical, Experimental and Clinical Principles, New York: Hodder Arnold, 2011.

[68] A. Razavi, E. Shirani and M. R. Sadeghi, "Numerical simulation of blood pulsatile flow in a stenosed carotid artery using different rheological models," *Journal of biomechanics,* vol. 44, no. 11, pp. 2021-2030, 2011.

[69] H. Wright, "Requirements to theses submitted in the Faculty of Engineering," Sydney, 2019.

[70] P. Poncin, C. Millet, J. Chevy and J. L. Proft, "Comparing and optimizing Co-Cr tubing for stent applications," *Proceedings of the materials and processes for medical devices conference,* pp. 279-283, 2004.

[71] ASM International, "Co-20Cr-15W-10Ni," *Materials and Coatings for Medical Devices Cardiovascular: MPMD Materials and Processes for Medical Devices,* pp. 69-73, 2009.

[72] A. Senthurnathan, "Computational and Experimental Assessment of the Mechanical Performance of Stents," Sydney, 2020.

[73] A. Idziak-Jabłońska, K. Karczewska and O. Kuberska, "Modeling of mechanical phenomena in the platinum-chromium coronary stents.," *Journal of Applied Mathematics and Computational Mechanics,* vol. 16, no. 4, pp. 29-36, 2017.

Appendices

Appendix A: Contribution to Journal Submission

This work directly contributed to the journal submission 'A Multi-Objective Hemodynamic Optimization of Stent Geometries' that is led by Dr Susann Beier. The title page is pictured in Figure 38 where I am a contributing author.

A Multi-Objective Hemodynamic Optimization of Stent Geometries

Ramtin Gharleghi[a], Heidi Wright[a], Vanesssa Luvio[a], Nigel Jepson[b,c], Anushan Senthurnathan[a], Behzad Babaei[a], Gangadhara Prusty[a], Tapabrata Ray[d], Susann Beier[a,*]

[a]*School of Mechanical and Manufacturing Engineering, University of New South Wales, High St. Sydney, Australia*
[b]*Prince of Wales Hospital, 320-346 Barker St. Randwick, Sydney, Australia*
[c]*Prince of Wales Clinical School of Medicine, 18 High St, University of New South Wales, Sydney, Australia*
[d]*School of Engineering and Information Technology, University of New South Wales, Canberra, Australia*

Abstract

Stents are scaffolding cardiovascular implants used to restore blood flow in narrowed arteries. However, the presence of the stent alters local blood flow and shear stresses on the surrounding arterial wall, which can cause adverse tissue responses and increase the risk of adverse outcomes. There is a need for optimization of stent designs for hemodynamic performance. We used multi-objective optimization to identify ideal combinations of design variables by assessing potential trade-offs based on common hemodynamic indices associated with clinical risk. We studied seven design variables including strut cross-section, strut dimension, strut angle, cell alignment, cell height, connector type and the connector arrangement. Optimization objectives were the percentage of vessel area exposed to adversely low and high Wall Shear Stress (WSS) and adversely low time averaged WSS (TAWSS), assessed using computational fluid dynamics modeling. Two multi-objective optimization algorithms were used to iteratively predict ideal designs. Out of 50 designs, three best designs with respect to each of the three objective, and two designs in regard to overall performance were identified. These designs are presented and discussed in the context of their trade-offs, similarity and difference to existing commercially available designs.

Keywords: stent design, computational modeling, wall shear stress

Figure 38. Contributing Author for Journal Submission.

Appendix B: Future Work Sample

Table 9 outlines the specific design variables chosen for the Latin Hypercube sample of 60 stents generated for future work. In Table 9, ^ represents an invalid design, R refers to a rectangular cross-section, and C refers to a circular cross-section. For the Number of Connectors (NC), '1' represents two connectors per cell, '2' represents three connectors per cell, and '3' represents the connector arrangement where there are three connectors in the first three proximal cells and two connectors per cell follow. For the Connector Type (CT), '1' represents straight, '2' represents spline, '3' represents S-shape, '4' represents M-shape, '5' represents alternating straight and spline, and '6' represents alternating straight and M-shape connectors. For the stent material, '1' represents platinum chromium, and '2' represents L-605 cobalt-chromium. The remaining variables are explained in Table 7 in Section 6.1.1.

Table 9. Sample of 60 Stents for Future Work.

#	CS	SD1 (μm)	SD2 (μm)	SA (°)	AT (°)	CH (mm)	CT	NC	Material	NP
00	R	103.4329	73.5277	43.5563	0	1.0796	1	1	2	7
01	R	98.9121	114.0338	40.5313	0	1.4072	1	2	1	8
02	R	76.3764	106.4540	38.5871	0	1.4346	5	3	2	9
03	R	85.0107	82.2091	47.6930	1	1.5574	3	1	2	9
04	R	73.6688	78.9438	46.1956	0	1.8002	1	2	2	6
05^	R	91.8221	85.5172	35.3836	1	0.8789	2	2	2	8
06	R	61.0140	98.0322	46.6667	0	1.9624	4	3	1	7
07	R	96.0836	88.1784	33.8580	1	1.8792	3	1	1	8
08	R	75.5467	113.0390	48.4227	0	0.9779	6	1	1	9
09	R	78.9049	109.5428	29.8744	1	1.8887	4	2	1	7
10	R	89.8238	103.1376	25.9217	1	1.7584	2	1	1	7
11	R	105.0973	69.2221	27.2961	0	1.3137	5	3	1	8
12	R	66.8697	74.3071	45.1135	1	1.4770	5	1	2	6
13^	R	86.2830	71.5121	39.3603	1	1.1614	3	3	1	6
14	R	71.2511	77.8114	36.0450	1	1.5970	5	3	1	7
15	R	69.8228	86.0863	49.7378	0	1.5062	6	1	2	6
16	R	95.4103	96.7800	25.1680	0	1.1946	3	2	2	6
17	R	119.4689	62.8580	44.9792	1	1.3578	2	1	2	9
18	R	83.0726	101.9313	30.5181	0	1.7017	2	2	2	6
19	R	108.9236	65.4354	34.9545	1	1.0035	1	2	2	9
20	R	93.0360	90.1483	38.2892	0	1.2305	4	2	1	9
21	R	106.9874	94.9763	41.4905	0	1.8156	3	3	1	7
22	R	101.0025	81.2326	32.1196	1	1.6165	6	1	2	9
23	R	111.8791	105.1243	42.2002	1	0.8428	5	3	2	8
24^	R	115.8833	110.0207	31.5089	1	1.1236	6	2	1	7
25	R	81.2560	93.0128	36.9809	1	1.9269	2	3	1	8
26	R	116.3703	117.6917	33.1155	0	1.6771	4	3	2	8
27	R	65.9345	60.0074	43.1682	1	1.0299	4	3	1	6
28	R	112.7902	66.0528	28.7504	0	0.9275	1	1	1	7
29	R	63.0028	119.7051	28.3286	0	1.2647	6	2	2	9

30	C	88.8060	-	40.0351	1	0.9247	4	1	2	9
31	C	71.6524	-	31.5495	1	1.7778	2	3	2	8
32	C	98.3801	-	27.5667	0	1.2851	4	1	2	6
33	C	81.0152	-	48.0436	1	1.7193	3	1	1	8
34^	C	94.9112	-	30.7681	1	1.2185	4	1	1	7
35	C	110.2649	-	28.6889	1	1.9878	6	3	2	6
36	C	92.6029	-	36.2103	0	1.3246	3	3	2	6
37	C	104.2421	-	42.1020	1	1.0045	6	3	1	8
38	C	78.3392	-	32.3185	0	0.8704	1	3	2	7
39	C	97.1312	-	49.6689	1	1.4184	3	1	1	8
40	C	84.3212	-	29.6965	0	1.0773	2	1	1	7
41	C	65.3168	-	44.3330	1	1.2493	3	1	1	7
42	C	119.9258	-	47.0632	1	1.1119	4	3	1	9
43	C	69.7263	-	25.5804	0	1.3741	1	3	1	8
44	C	72.3477	-	46.0239	0	1.1804	5	2	2	9
45	C	108.3337	-	37.4400	1	1.6806	1	1	2	9
46	C	60.3106	-	49.0600	0	1.8941	1	2	1	6
47	C	76.8621	-	34.7042	0	0.8637	5	2	1	6
48	C	116.0588	-	33.5477	0	1.3832	3	1	2	7
49	C	87.9848	-	33.1484	1	1.8829	5	2	2	9
50	C	66.7363	-	38.5765	0	1.5458	5	3	1	7
51	C	113.5975	-	39.2345	1	1.9508	6	2	2	9
52	C	63.3946	-	45.7250	0	1.4666	2	3	2	9
53	C	91.9593	-	26.0884	0	1.5075	2	1	2	6
54	C	74.4633	-	37.8741	1	0.9558	6	2	1	7
55	C	115.2151	-	35.1428	1	1.0531	6	2	2	8
56	C	100.2671	-	42.7850	1	1.6353	1	2	1	8
57	C	102.2233	-	41.4257	0	1.5833	4	2	1	6
58	C	82.9790	-	43.8193	0	1.8052	2	3	1	7
59	C	106.0402	-	26.7036	0	1.7432	5	2	2	8